Ecological Modelling 481 (2023) 110367

Contents lists available at ScienceDirect

Ecological Modelling

journal homepage: www.elsevier.com/locate/ecolmodel

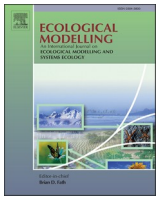

Burning trees in frozen soil: Simulating fire, vegetation, soil, and hydrology in the boreal forests of Alaska

Melissa S. Lucash [a,1,*], Adrienne M. Marshall [b], Shelby A. Weiss [a,c], John W. McNabb [d], Dmitry J. Nicolsky [e], Gerald N. Flerchinger [f], Timothy E. Link [g], Jason G. Vogel [h], Robert M. Scheller [i], Rose Z. Abramoff [j], Vladimir E. Romanovsky [e]

[a] Department of Geography, 1251 University of Oregon, 97403 Eugene, OR, USA
[b] Hydrologic Sciences and Engineering Program, Colorado School of Mines, 80401 Golden, CO, USA
[c] National Great Rivers Research and Education Center, 1 Confluence Way, East Alton, IL, USA
[d] Intel Corporation, 2200 Mission College, Blvd, 95054 Santa Clara, CA, USA
[e] Geophysical Institute, University of Alaska Fairbanks, 903 Koyukuk Drive, 99775 Fairbanks, AK, USA
[f] USDA Agricultural Research Service Northwest Watershed Research Center, 251 E. Front Street, Suite 400, 83702 Boise, ID, USA
[g] Department of Forest, Rangeland, and Fire Sciences, University of Idaho, 875 Perimeter Drive, 83844 Moscow, ID, USA
[h] School of Forest, Fisheries and Geomatics Sciences, University of Florida, 32611 Gainesville, FL, USA
[i] Department of Forestry and Environmental Sciences, North Carolina State University, 27695 Raleigh, NC, USA
[j] Lawrence Berkeley National Laboratory, 94720 Berkeley, CA, USA

ARTICLE INFO

Keywords:
Boreal forest
Forest simulation model
Hydrology
LANDIS-II
Permafrost
Wildfire

ABSTRACT

Boreal ecosystems account for 29% of the world's total forested area and contain more carbon than any other terrestrial biome. Over the past 60 years, Alaska has warmed twice as rapidly as the contiguous U.S. and wildfire activity has increased, including the number of fires, area burned, and frequency of large wildfire seasons. These recent and rapid changes in climate and wildfire have implications for future vegetation composition, structure, and biomass in interior Alaska, given that the vegetation is highly dependent on active layer thickness, soil moisture, organic layer depth, and plant-available nutrients. Here we developed a new succession extension (DGS) of the LANDIS-II forest landscape model which integrates a vegetation dynamics model (NECN) with a soil carbon model (DAMM-McNiP), a hydrologic model (SHAW), and a deep soil profile permafrost model (GIPL) in a spatially-explicit framework. DGS Succession uses the algorithms in the NECN Succession extension of LANDIS-II to simulate growth, mortality and reproduction of vegetation but has three major improvements. First, the simple bucket model in NECN was replaced with a physically-based model (SHAW) that simulates energy and water fluxes (e.g. snow depth, evapotranspiration, soil moisture) at multiple levels in the canopy and soil. Second, the active, slow, and passive soil pools in NECN were replaced by seven soil pools that are measurable in the field, with carbon and nitrogen dynamics dictated by DAMM-McNiP. Finally, soil temperature and soil moisture are simulated only at one depth in NECN, but in DGS, soil temperature (and hence permafrost dynamics) are simulated at as many as 50 user-defined depths down to 4 m with SHAW and 75 m with GIPL. During the initial calibration phase, DGS was applied at three inventory sites at the Bonanza Creek Long Term Ecological Research area in Interior Alaska where climate forcings, species biomass, soil temperature, and/or soil moisture were available. For the landscape-scale simulations, DGS was run with the SCRPPLE fire extension of LANDIS-II under two scenarios of climate using a ~400,000 ha landscape that included the inventory sites. Across all three sites, DGS generally captured the variation in soil moisture and temperature across depths, seasons, and years reasonably well, though there were some discrepancies at each site. DGS had better agreement with field measurements of soil moisture and temperature than its predecessor NECN which produced unrealistically low soil moisture and unrealistically high seasonal fluctuations in soil temperature. At the landscape scale, ignitions, area burned, and soil temperature increased under climate change, as expected, while soil moisture was relatively unchanged across climate scenarios. Biomass tended to decline under climate change, which differs from other modeling studies in this region but is consistent with the browning trends observed from remote sensing

* Corresponding author.
E-mail address: mlucash@uoregon.edu (M.S. Lucash).
[1] Current affiliation: Department of Geography, 1251 University of Oregon, 97403-1251 Eugene, OR, USA.

https://doi.org/10.1016/j.ecolmodel.2023.110367
Received 13 December 2022; Received in revised form 13 March 2023; Accepted 20 March 2023
Available online 31 March 2023

data. Simulating climate, vegetation succession, hydrology, permafrost, carbon and nutrient cycling, and wildfire in an integrated, spatially-explicit framework like LANDIS-II will allow us to disentangle the drivers and ecosystem responses in this rapidly changing ecosystem, as well as other forested systems with complex hydrologic, biochemical, cryospheric, and vegetation feedbacks.

1. Introduction

Boreal ecosystems stretch approximately 16 million km^2 around the northern portion of the globe, accounting for 29% of the world's total forested area (UN-ECE/FAO, 1985). They contain 1041 Pg of C (median, range of 367–1715 Pg), more carbon than any other terrestrial biome (Bradshaw and Warkentin, 2015). Their sheer size and C storage capacity make them important, but it is their recent, rapid climatic changes and potential fragility that foster particular interest in these high latitude regions, such as Alaska.

Over the past 60 years, Alaska has warmed twice as rapidly as the contiguous U.S. (Markon et al., 2018; Overland et al., 2018) and current temperatures are unprecedented in the last 100–400 years (Barber et al., 2004; Overpeck et al., 1997). Temperatures have warmed most dramatically in the winter (Wolken et al., 2011), resulting in a decline in the snow season length by about 2.5 days per decade (Euskirchen et al., 2007, 2006). Temperatures have also warmed in the spring and fall; an earlier spring start and a slightly later date of the first frost in the fall have resulted in a 45% increase in growing season length over the past 91 years (Wendler and Shulski, 2009). Projections indicate that warming will continue to outpace lower latitudes and temperatures will increase by another 2–8 °C by the end of the century (Leonawicz et al., 2015) Late-century projections (CCSM4 RCP8.5) suggest the snow season will decline by ~28 days (Lader et al., 2020) and the lengthening of the growing season will increase by almost 50 days in Alaska, as compared to only 30–40 days in the contiguous United States (Lader et al., 2017; Walsh, 2014). Precipitation has shown very little change (Bieniek et al., 2014), and studies that do find an observed precipitation change disagree on the direction (Hinzman et al., 2005; L'Heureux et al., 2004; McAfee et al., 2013) in Alaska over the past century. Precipitation in Alaska is projected to increase over the next century, given that warmer air has a higher holding capacity for water vapor, but the uncertainty is high, ranging from 10% to 50% depending on the model and emissions scenario (Bieniek et al., 2014; Tebaldi et al., 2004). Maximum daily precipitation is expected to increase by 53% by 2100, which far exceeds the estimates for the contiguous United States which range from 10% to 40% (Lader et al., 2017). The ratio of snow to total precipitation is projected to decrease from ~44% to 21% under the CCSM3 and GFDL-CM3 climate scenarios by the end of the late-century (Lader et al., 2020).

Interior Alaska, bounded by the Alaska Range (~63°N) to the south and the Brooks Range (~67°N) to the north, is dominated by upland and lowland boreal forests. White spruce (*Picea glauca* (Moench) Voss) was the first conifer to expand in interior Alaska 10,000 years BP, and it dominated the region for much of the mid-Holocene (10,000 – 5000 years BP, Edwards et al., 2005). As the climate became cooler and moister, black spruce (*Picea mariana* (Mill.) Britton, Sterns & Poggenb.) increased in abundance (Higuera et al., 2009a; Lynch et al., 2003a) and now covers about 40% of boreal Alaska (Van Cleve et al., 1983). Interior Alaska also supports prevalent deciduous broadleaf trees, such as trembling aspen (*Populus tremuloides* Michx.), Alaskan paper birch (*Betula neoalaskana* Sarg.), and balsam poplar (*Populus balsamifera* L.).

Wildfire is the primary disturbance in the boreal forests of Alaska and around the world now (Payette, 1992) and for the past thousands of years (Higuera et al., 2009b; Hoecker et al., 2020; Kelly et al., 2013; Lynch et al., 2003b). Climate warming has increased fire activity in the circumboreal forest (M. D. Flannigan et al., 2009; Lynch et al., 2003) and in Alaska (Calef et al., 2015; Duffy et al., 2005), including a 50% increase in overwintering (aka zombie) fires (Scholten et al., 2021). The average number of fires per year in Alaska has expanded from 125 in the 1940′s to >461 in the 2000′s (Hinzman et al., 2013). Ignition density has increased by 4.8% each year since 1975 (Veraverbeke et al., 2017). This is due, in part, to increases in the length of the fire season, with significant increases in the number of days with lightning ignitions since the late 1950′s in boreal North America (Coogan et al., 2020). Area burned doubled from the 1960s/1970s to the 1980s/1990s in boreal North America (Kasischke and Turetsky, 2006) and increased by 4.6-fold in interior Alaska since 1943 (Calef et al., 2015). In some areas of Alaska, the fire return interval has decreased from 120 - 1100 years (Johnstone et al., 2010a; Van Cleve and Viereck, 1981) to less than 50 years (Brown and Johnstone, 2012; Johnstone and Chapin, 2006). As wildfire activity increases in Alaska, it becomes more important than ever to use fire simulators that capture the temporal resolution, spatial interactivity, vegetation, and climate integration necessary to capture future changes in the fire regime. Some fire models use monthly (e.g. TEM, Balshi et al., 2009) rather than daily data to capture ignition rates, do not simulate fire spread from one raster pixel to another (e.g. UAFME, Foster et al., 2019; MC1, Bachelet et al., 2005), omit shrubs, mosses and lichen as fuel types (e.g. FVS-FFE, Rebain, 2010), or rely on user-defined fire return interval (e.g. UAFME, Foster et al., 2019), preventing climate-driven changes in intervals. Models like Scrpple (Scheller et al., 2019) that use daily data, simulate fire spread using cell automata, recognize that understory species as important fuel types, and have a tight coupling to climate without fixed fire return intervals, can aid in predicting future changes in wildfire regimes under a changing climate.

Changes in the wildfire regime in Alaska have started to break the 6000 year "legacy lock" of spruce domination (Hoy et al., 2016; Johnstone et al., 2010b), increasingly favoring hardwood species with longer dispersal distances and shorter times to sexual maturity. Black spruce has seeding distances less than 1 km, whereas aspen and birch can disperse several kilometers from the parent tree (Burns and Honkala, 1990; Marquis et al., 1969; McCaughey et al., 1986). Also, as the prevalence of short-interval fires increase in Alaska (Buma et al., 2022), sites can suffer from immaturity risk, because the fire-free periods are too short for conifer seed production (Keeley et al., 1999). Black spruce has low rates of seed production and cone serotiny until it reaches sexual maturity (>30 years old, (Buma et al., 2013; Burns and Honkala, 1990) and often requires at least 50 years to accumulate sufficient seed for stand self-replacement after fire (Viglas et al., 2013). In contrast, alder, quaking aspen and paper birch initiate seed production at 5, 10, and 15 years old, respectively. Germination success and recruitment rates also influence the effectiveness of conifer self-replacement. A long fire return interval allows sufficient time for the thick organic seedbeds to develop, which present a barrier for small deciduous seeds (but not larger-seeded conifers) to reach the stable moisture supply in the mineral soil (Hesketh et al., 2009). However, sites with short-interval fires have thinner organic layers and more exposed mineral soil (Shabaga et al., 2022), which favors deciduous species like aspen (Jasinski and Payette, 2005; Johnstone and Chapin, 2006). Many models represent vegetation as broad vegetation types (AFRESCO, TEM, ecosys) and do not simulate seed dispersal or vegetative reproduction (e.g. TEM), which may not fully capture the species-level traits and reproductive strategies that determine long-term successional trends.

In the boreal forests of interior Alaska, forest type, wildfire, and soil moisture are the most important agents controlling the thickness of the organic horizon (Johnstone et al., 2010a), which is the primary determinant controlling the aggradation or degradation of permafrost (Viereck, 1982). Permafrost, soil with a temperature at or below 0 °C for

at least two consecutive years, underlies approximately 75–80% of the ground in interior Alaska (Osterkamp and Romanovsky, 1999). Cooler and wetter areas, such as north-facing and toe-slope forests, are more likely to contain permafrost than warmer and drier south-facing slopes (Hinzman et al., 2006). Shallow permafrost and thick organic horizons are often associated with black spruce forests and lowlands, where soils are moist because evapotranspiration rates are low due to low productivity (Bonan, 1991; Liu et al., 2005), decomposition is low due to anoxia and cold temperatures (Hobbie et al., 2000; Schimel and Clein, 1996), and mosses are prevalent and have high water retention capacity (Turetsky et al., 2010). Broadleaf forests, more prevalent on warm, well-drained soils, often have thinner organic horizons and less moss understory (Natalia et al., 2008; Van Cleve and Viereck, 1981), due to higher evapotranspiration and decomposition rates associated with higher productivity (Bonan, 1991; Liu et al., 2005), thereby causing greater fluctuations in summer temperatures, and lacking permafrost. Most permafrost models, like GIPL2, capture the effects of forest type on permafrost (Nicolsky et al., 2009), but lack dynamic vegetation, wildfire, and hydrology modules that capture potential changes in species composition, wildfire, and soil moisture that drive long-term changes in permafrost.

Wildfire also influences permafrost, through its effects on surface energy balance. Following wildfire, the thickness of the organic horizon is reduced, causing a significant increase in the thermal conductivity of soil and an increase in active layer thickness, the portion of the soil above the permafrost that thaws and freezes seasonally (Jafarov et al., 2013). Permafrost tends to return 20–30 years after low-severity fire as the forest floor begins to develop and mosses regain dominance (Bernhardt et al., 2011; Viereck et al., 2008). In areas with high severity fire where larger amounts of the surface organic material are combusted, permafrost may disappear from the upper few meters of soil (Yoshikawa et al., 2003). Across interior Alaska, permafrost soils are often right at the cusp of thawing, with temperatures usually ranging from –0.1 to –3.5 °C (Jorgenson et al., 2010; Osterkamp and Romanovsky, 1999), due in part to recent climate warming (Hinzman et al., 2006; Osterkamp and Romanovsky, 1999). Rising temperatures in Alaska are likely to cause longer fire seasons (Jolly et al., 2015; Kasischke et al., 2010) and increases in the frequency and severity of fires (H. Genet et al., 2013; Kasischke et al., 2010) which can cause permafrost thaw (Nicolsky et al., 2007). Also, as temperatures rise and fire frequency increases, active layer thickness increases and the depth to permafrost increases, enabling soil water to drain deeper into the soil profile. Recent warming has also caused earlier snowmelt and later freeze-up, which have lengthened the growing season in interior Alaska (Sharratt, 1992), and increased the potential for drought (Barber et al., 2000), especially when coupled with the changes in depth to permafrost and hence altering wildfire dynamics.

Recent efforts to quantify the effects of climate change and wildfire on boreal Alaska have specifically highlighted the need to improve our understanding of the interactions between climate, fire, vegetation, hydrology, and soils (Alexander and Mack, 2016; A.C. Foster et al., 2019; Rogers et al., 2015). In the past, ecosystem models, such as ALFRESCO, TEM, ecosys, UVAFME, and iLAND, have been used to simulate climate-vegetation-fire interactions in Alaska (Euskirchen et al., 2009; H. Genet et al., 2013; Mekonnen et al., 2019; Rupp et al., 2007), but they have several limitations. For example, AFRESCO, TEM, and ecosys classify vegetation into vegetation types and therefore do not capture species' competitive dynamics. Individual-based gap models, like UVAFME (University of Virginia Forest Model Enhanced), are able to capture species dynamics in interior Alaska, but they do not simulate spatially-interactive processes like seed dispersal and wildfire spread (Foster et al., 2022a, A.C. 2019). The model iLAND simulates spatially-interactive species growth, tree dispersal, and wildfire spread at the individual tree level (Hansen et al., 2021), but it primarily focuses on aboveground processes with soil moisture simulated for a single layer using a simple bucket model (Seidl et al., 2012). UVAFME simulates soil moisture at two depths (organic and mineral layers) (A.C. Foster et al., 2019), whereas TEM, ALFRESCO-TEM, and ecosys simulate soil moisture at multiple depths, including the depth of the water table (Dimitrov et al., 2010; Yi et al., 2009). Permafrost dynamics are captured in all these models, except iLAND. UVAFME (A.C. Foster et al., 2019), DOS-TEM (Genet et al., 2013), and ecosys (Mekonnen et al., 2019) simulate the effects of wildfire on the depth of burn, though in ecosys it is a spatially homogenous, user-defined input.

In this paper, we describe a new succession extension (Damm/mcnip-Gipl-Shaw, henceforth 'DGS') of the LANDIS-II forest landscape model (Scheller et al., 2007) that greatly expands our ability to simulate climate, species-level succession, hydrology, permafrost, carbon and nutrient cycling, and wildfire in a spatially-explicit framework. DGS Succession uses the algorithms in the NECN (Net Ecosystem Carbon and Nitrogen) Succession extension of LANDIS-II to simulate growth, mortality, and reproduction of vegetation, but the potential drivers of growth (e.g. soil temperature, available soil moisture, and available nitrogen) were updated. The simple water bucket model in NECN was replaced with a physically-based model (Simultaneous Heat And Water balance model; SHAW; Flerchinger et al., 2016a; Flerchinger and Cooley, 2000; Flerchinger and Saxton, 1989) that simulates energy fluxes (e.g. direct and diffuse solar radiation, albedo, heat transfers within snowpack) and water fluxes (e.g. snow accumulation and ablation, evapotranspiration, soil moisture) at multiple strata in the canopy and up to 49 user-defined depths in the soil down to 4 m. The active, slow, and passive soil pools in NECN were replaced by seven soil pools that are measurable in the field (soil organic C and N, dissolved organic C and N, microbial biomass C and N, and extracellular enzymes), with carbon and nitrogen dynamics dictated by the algorithms in the DAMM-McNiP (Dual Arrhenius Michaelis-Menton Carbon and Nitrogen Physiology) model (Abramoff et al., 2017a). A deep soil profile permafrost model (Geophysical Institute Permafrost Laboratory; GIPL version 2.0; (Nicolsky et al., 2009) was integrated into DGS to simulate soil temperature at up to 50 user-defined depths down to 75 m. Recoding these published models of soil C, hydrology, and permafrost from FORTRAN (SHAW and GIPL) and R (DAMM) to the C# framework of LANDIS-II, enabled us to simulate integrated, dynamic responses and spatially-explicit feedbacks using models that were already well-established and fully-vetted. The DGS extension was calibrated using four sites in interior Alaska and then used to simulate current and future vegetation, hydrology, and permafrost in a 397,860 hectare landscape in interior Alaska at a 200 m × 200 m grid resolution. In this paper, our objective was to assess how soil moisture, soil temperature, vegetation, and soil C may be altered by climate change and illustrate how the future dynamics of Alaskan ecosystems can be simulated using DGS, a tightly coupled model of climate, vegetation, soil (including organic layers and permafrost), hydrology, and wildfire.

2. Methods

2.1. Model overview

Our new succession extension (described below) was integrated within LANDIS-II, an open-source, spatially-explicit, process-based simulation framework that is optimized for large-scale spatial dynamics (Scheller et al., 2007). In LANDIS-II, the landscape consists of interconnected grid cells; each cell contains species-age cohorts of trees and is assigned to a climate region, within which climate is assumed to be homogenous (Mladenoff, 2004). Tree growth and mortality are not spatially interactive (i.e. competition between cohorts occurs within a cell), but reproduction (e.g. seed dispersal) and disturbances are spatially-interactive. This robust framework allows multiple ecological processes (e.g., growth, mortality, regeneration, decomposition, and disturbances) to change in space and time, allowing for potential overlap to capture interactions between processes (Scheller et al., 2007). LANDIS-II has been widely adopted for use in climate change research in

the boreal forests of Siberian Russia (Gustafson et al., 2011, 2010), British Columbia (Dymond et al., 2016), and Newfoundland-Labrador (Sturtevant et al., 2009).

DGS (pronounced "digs") was created to improve the simulation of forest dynamics in the boreal region of western North America. DGS integrates climate, vegetation, permafrost, and hydrology within a spatially-explicit framework that interfaces with an existing wildfire extension which simulates ignitions, spread, and severity (Fig. 1). All model code is available at: https://github.com/LANDIS-II-Foundation/Extension-DGS-Succession and information about inputs and outputs are provided in the associated user guide. Model inputs used for this study are available at: https://github.com/LANDIS-II-Foundation/ReburnsAK/.

2.2. Climate

The LANDIS-II climate library (Lucash and Scheller, 2021), which processes the climate input data for LANDIS-II, was modified to add specific humidity and shortwave radiation as input variables because they are required for SHAW's energy and water balance algorithms (Lucash and Scheller, 2021). An algorithm to convert specific humidity to dewpoint temperature was also added (American Meteorological Society, 2020).

2.3. Aboveground vegetation dynamics

DGS Succession uses the algorithms in the NECN Succession extension of LANDIS-II (Scheller et al., 2012, 2011) to simulate monthly forest above- and belowground plant growth and associated carbon (C) and nitrogen (N) cycling. DGS simulates aboveground (leaves and wood) and belowground (fine and coarse roots) productivity of each cohort on each raster cell. To calculate cohort growth within a cell, it uses species-specific life history attributes (e.g., longevity, shade tolerance), climate, age, competition (i.e., the biomass of other cohorts relative to the amount of maximum potential biomass), water availability, N availability, and soil temperature. While DGS simulates growth, mortality and reproduction of vegetation with the same algorithms as NECN, the computations for water availability, nitrogen availability and soil temperature are different. NECN relies on the simple water bucket model of CENTURY (Parton et al., 1994, 1988) to compute soil moisture, but DGS uses a physically-based model (SHAW) that simulates simultaneous energy and water fluxes, including soil moisture dynamics at multiple depths in the soil (see below). Nitrogen availability is also calculated differently in DGS; the algorithms in NECN CENTURY were replaced with DAMM-MCNiP (see below). CENTURY uses a simple algorithm to derive soil temperature from air temperature, but DGS uses GIPL, which solves a nonlinear heat flow equation to calculate soil temperature at multiple depths in the soil (see below). As in NECN, DGS simulates tree mortality caused by senescence (ongoing loss of trees and branches), age (to account for the increase in mortality as a species approaches its life expectancy), and disturbances (described below). It also simulates regeneration via seeds, serotiny, or re-sprouting using life history attributes. Regeneration in DGS is identical to NECN (Scheller et al., 2007) except that the water available for seedlings to regenerate is calculated by SHAW (see below).

2.4. Belowground soil dynamics

Soil carbon dynamics in NECN were derived from CENTURY (Parton et al., 1994, 1988). In DGS, CENTURY was replaced by DAMM-MCNiP (Abramoff et al., 2017), a new hybrid model of DAMM (Dual Arrenius Michaelis Menton) (Davidson et al., 2014, 2012) and Microbial Carbon and Nitrogen Physiology Model (MCNiP), described in (Finzi et al., 2015). In contrast to CENTURY which measures carbon and nitrogen cycling in theoretical (active, slow, and passive) soil pools, DAMM-McNiP explicitly simulates measurable C and N pools and fluxes in soil using physiological principles with relatively low parameter collinearity (Abramoff et al., 2017).

DAMM-McNiP tracks seven pools: soil organic C (SOC) and N (SON), dissolved organic C (DOC) and N (DON), microbial biomass C and N, and extracellular enzymes (Abramoff et al., 2017). Litter inputs are partitioned evenly between soil organic matter (SOM) and dissolved organic matter (DOM) pools each month for both C and N. Soil CN pools are responsive to changes in soil temperature, soil moisture, oxygen concentrations, and substrate CN stoichiometry. Temperature affects the rate of SOM depolymerization to DOM using Arrhenius kinetics. Soil water content modifies the supply of oxygen and DOM, both of which affect depolymerization using a Michaelis Menten (M-M, i.e., dual Monod) kinetic approximation. Oxygen concentration limits the depolymerization rate when soil water content is high, while the litter inputs limit depolymerization when soil water content is low, because the substrate cannot diffuse to the reaction site. Microbial uptake is limited by both DOC and DON substrate and oxygen concentration using M-M kinetics with uptake partitioned in the microbial pool among maintenance, growth, and enzyme production. Enzyme production can be limited by stoichiometry of microbial C or N. All model pools and fluxes are calculated internally within the model; DGS outputs are SOC and SON, DOC and DON, inorganic N, respiration and N mineralization.

2.5. Hydrology

Within the DGS extension, SHAW simulates energy and water fluxes

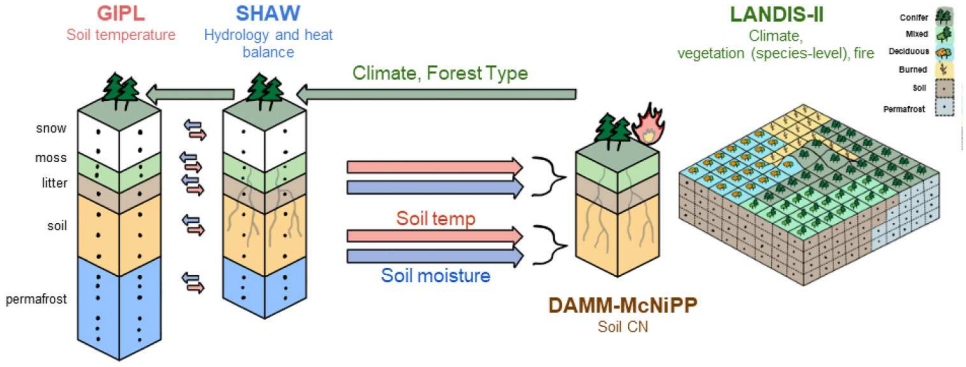

Fig. 1. Description of the models integrated within the DGS extension of LANDIS-II. DGS simulates (1) climate and vegetation dynamics, including tree and shrub growth, mortality, and reproduction, (2) soil carbon and nitrogen dynamics with DAMM-McNiP, (3) hydrology and heat balance (e.g. snow depth, evapotranspiration, soil moisture) at multiple levels in both the canopy and soil using the SHAW model, and (4) soil temperature (i.e. permafrost dynamics) down to 75 m using GIPL. DGS succession can be run with any of the existing LANDIS-II fire extensions, including SCRPPLE, the newest fire extension of LANDIS-II that simulates lightening fires, human accidental fires and prescribed fires (Scheller et al., 2019). The models within DGS have a consistent climate stream and are coupled whereby GIPL simulates soil temperature at user-defined depths down to 75 m and provides the values to SHAW, which simulates soil moisture at depths down to 30 m. Tree-available soil moisture and temperature from SHAW and GIPL influence successional dynamics, such as vegetation growth and species composition, and soil carbon and nitrogen dynamics.

through the vertical soil-vegetation-atmosphere continuum (Flerchinger et al., 2016a; Flerchinger and Cooley, 2000; Flerchinger and Saxton, 1989), accounting for the effects of snow, surface vegetation, and litter on subsurface water and energy dynamics. At a daily time step, SHAW simulates: 1) snow accumulation and ablation of a multi-layer snowpack using a complete energy balance (Flerchinger et al., 1994), 2) surface runoff and infiltration using the Richard's equation for unsaturated flow (Richardson, 1922), 3) evapotranspiration using gradient flow through a multi-layer canopy (Flerchinger et al., 2016b), and 4) transpiration governed by user-defined vegetation structural and water use characteristics, including Jarvis-Stewart type controls of stomatal resistance (Armatas et al., 2018; Jarvis, 1976; Stewart, 1988). SHAW has been used to simulate water and energy transfer through forest and shrub canopies for a wide range of climate and vegetation conditions in complex terrain (Chauvin et al., 2011; Flerchinger et al., 2016c; Link et al., 2004; Marshall et al., 2019). It has also been used to simulate the effects of fire on a seasonally frozen system in southwestern Idaho (Flerchinger et al., 2016c), discontinuous permafrost at the Wolf Creek and Scotty Creek boreal research sites in Canada (Zhang et al., 2010), and soil moisture and temperature dynamics at multiple sites in interior boreal Alaska (Marshall et al., 2021b, 2021a). The strength of SHAW lies in its physically-based approach to simulating the coupled transfer of energy and water at a daily timestep, including soil moisture and soil temperature dynamics at up to 65 soil depths. However, the one-dimensional nature of SHAW means that DGS is most appropriately applied in areas where net lateral flows are minimal.

2.6. Permafrost dynamics

The GIPL model within DGS solves a nonlinear heat flow equation with phase change and has been specifically developed to simulate spatially distributed permafrost dynamics (Marchenko et al., 2008; Nicolsky et al., 2007; Sergueev et al., 2003) in a wide range of climatic conditions across Alaska (e.g., Debolskiy et al., 2020; Jafarov et al., 2012; Nicolsky et al., 2017). GIPL is forced by daily air temperature and snowpack conditions to simulate phase changes with prescribed accuracy. A special enthalpy-based formulation of the energy conservation law allows simulation of phase change processes without loss of latent heat effects (Nicolsky et al., 2009). Soil properties, including heat capacity and thermal conductivity were typically based on the water and ice content in the ground material in previous versions of GIPL, but in DGS, water and ice content are inherited from SHAW. Some water is assumed to remain liquid below 0 °C; its content is defined empirically according to the ground temperature (Romanovsky and Osterkamp, 2000). The modeling domain is discretized on a regular grid with ground thermal properties parameterized according to the dominant vegetation type of each cell (Nicolsky et al., 2017). The soil properties for each vegetation type are prescribed either by the data assimilation techniques or set according to published literature, and modeling results are typically vetted against soil temperature observations (Debolskiy et al., 2020; Nicolsky et al., 2017).

2.7. Wildfire

The SCRPPLE extension v. 2.3 for LANDIS-II was used to simulate the current and future wildfire regime (Scheller et al., 2019). SCRPPLE (Social-Climate Related Pyrogenic Processes and their Landscape Effects) uses a data-driven approach to simulating wildfire by using remotely-sensed fire databases to parameterize fire ignitions and daily fire spread in the model. This approach allows the user to capture landscape-scale determinants of fire behavior which are most appropriate to the scale of the LANDIS-II model. Fire regimes respond dynamically to changes in climate, including temperature, precipitation, wind direction, and wind speed.

Ignitions use a "supply and allocation" model whereby the probability of ignition is determined by an ignition probability surface derived from historical fires observed within the study landscape (Scheller et al., 2019) and model of historic daily ignitions by fire weather index fit to a zero-inflated Poisson distribution (Zuur et al., 2009). Fire spread to adjacent cells (i.e. the four nearest neighbors) is dependent on past spread occurrences of historic fires (Scheller et al., 2019). Specifically, the model creates a probability function for daily fire spread success at the cell-level based on daily fire perimeters, Fire Weather Index (FWI), fine fuels, and downscaled wind speed. Wind speed is downscaled from the climate region to the raster-scale by accounting for slope and azimuth relative to wind direction and the intensity of fire on neighboring cells. Fine fuels are calculated internally by DGS and are spatially and temporally variable. A fire will spread until it has reached its maximum daily spread area based on the relationship fit between daily fire spread areas and associated FWI and effective wind speed. Fire intensity (low, medium, high) is calculated based on the mass of fine fuels, mass of ladder fuels, and fire intensity of neighboring cells. Mortality is dependent on fire intensity, tree species, and tree ages. This data-driven approach uses the historical relationships between fuel, climate, and fire behavior to capture the important drivers of fire in the specified region, but it also allows future fire behavior to dynamically respond to projected climate and fuels.

2.8. Model integration of LANDIS-II, SHAW, GIPL and wildfire

SHAW and GIPL were recoded from FORTRAN to C# to allow for integration into the spatially-explicit LANDIS-II framework, adding an additional 18,093 lines of code to DGS. DGS assigns each raster cell to a Temperature-Hydrology Unit (THU), which can be delineated based on climate zone, elevation, slope, vegetation type, and time-since-fire (or more generally time-since-disturbance). Each THU has a corresponding series of input parameters determined by user-defined look-up tables for both SHAW and GIPL.

In each year of the simulation, DGS provides the climate, slope, aspect, vegetation type, and time-since-disturbance in each cell to the SHAW and GIPL submodules, which is used to determine the annual assignment of THUs across the entire landscape. In the first month of the simulation, DGS provides the climate data to GIPL which uses it to compute daily soil temperatures from the surface to the bottom of the soil profile for each THU. The GIPL soil temperature at SHAW's lower boundary depth (e.g. 4 m) is passed from GIPL to SHAW to specify SHAW's lower boundary conditions. Then SHAW computes soil moisture and soil temperature dynamics throughout its soil profile and passes the water content by depth to GIPL. In subsequent years, SHAW and GIPL consecutively trade temperature and water content at each depth for each month of the simulation. GIPL and SHAW provide soil temperature and available soil water, respectively, to the vegetation in DGS at two depths: integrated across the top 10 cm and integrated from 10 cm to the species-specific rooting depth, which is an input in the model. Available water and soil temperature are used by DGS with temperature and moisture response curves to determine how much water and soil temperature limit aboveground productivity at a monthly timestep.

Study Area

The study landscape contains 397,860 hectares in the greater Fairbanks area, nested within interior Alaska (Fig. 2). Black spruce covers 29% of the landscape, which often dominates on north-facing slopes (Van Cleve et al., 1986; Van Cleve and Viereck, 1981). Aspen (*Populus tremuloides*) occupies the warmer, drier south-facing sites with a thin organic horizon. Locations with microclimates and soil characteristics that are intermediate between black spruce and aspen are dominated by white spruce (*Picea glauca*) and birch (*Betula neoalaskana*) which cover 31% and 32% of the landscape, respectively. The region was not glaciated during the Pleistocene glaciation (Pewe et al., 1976) and is characterized by gentle sloping uplands. Soils are primarily silt loams, accrued from eolian deposition from the Alaska Range and fluvial plains during the Holocene (Black, 1951). The landscape is underlain by discontinuous permafrost, the presence of which is determined by

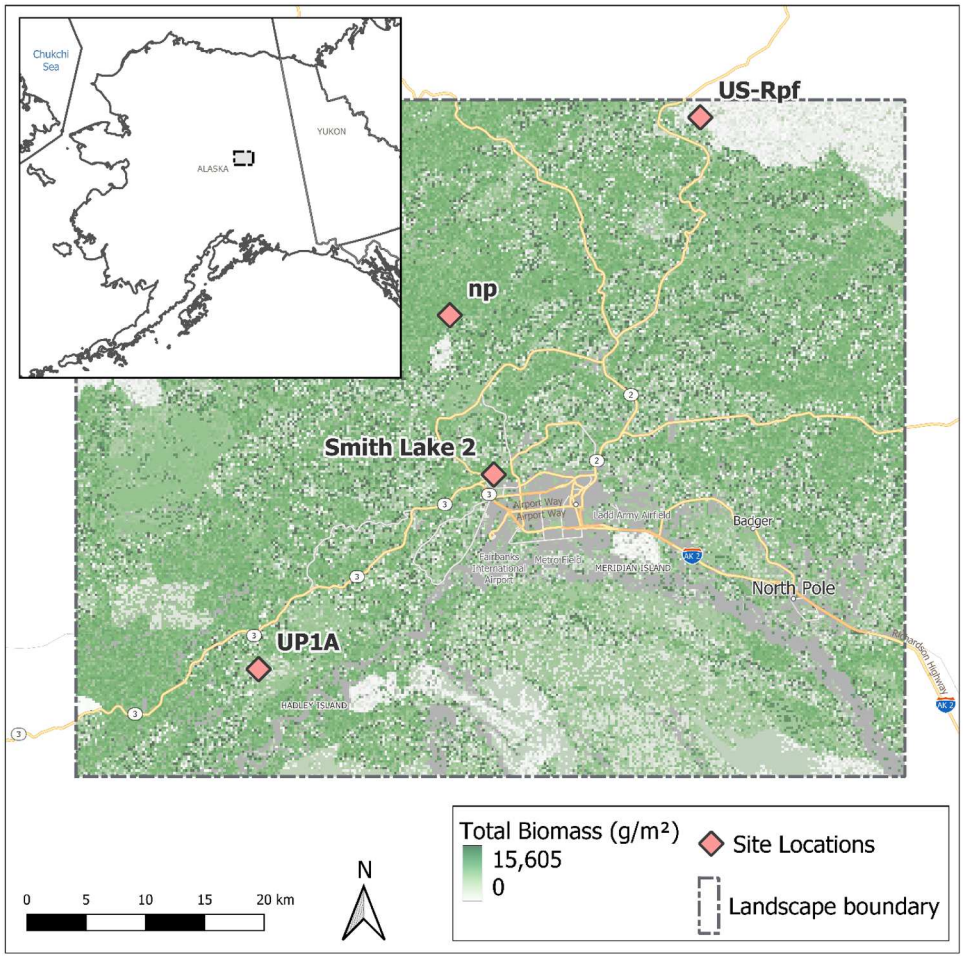

Fig. 2. Study landscape in interior Alaska as delineated by three Bonanza Creek LTER sites (US-Rpf, UP1A and Smith Lake 2) and one field study (np) used for calibration, encompassing an area of 397,860 hectares. Estimated total biomass (g biomass m^{-2}) at the start of the simulation is also shown, which reflects the initial vegetation map of species composition and species' age imputed from FIA data. Areas in gray indicate inactive cells (i.e., cells containing rivers, lakes, or human infrastructure).

vegetation type, disturbance history, and topography. Monthly mean air temperatures range from −19.4 °C in January to 15.9 °C in July, based on our analysis of gridded weather observations from 1981 to 2010 (PRISM Climate Group: Oregon State University, 2021). Mean annual precipitation is 358 mm with about half of precipitation occurring during the growing season.

Four previously established field sites were selected within the study landscape for site-scale model evaluation (Fig. 2), based on the availability of climate, soil moisture and temperature data, minimization of net lateral hydrologic fluxes (i.e. focusing on upland sites), and representation of post-fire successional trajectories. Two of our sites were dominated by deciduous species without near-surface permafrost, including a site (US-Rpf, 65.1198 °N, −147.4290 °W) burned in 2004, now dominated by birch and quaking aspen (*Populus tremuloides*) (Ueyama et al., 2019, 2018a) and a site (Bonanza Creek Long-Term Ecological Research UP1A, 64.7355 °N, −148.3027 °W) burned in 1983, now dominated by paper birch (*Betula papyrifera*) (van Cleve et al., 2015a). Our coniferous site (Ameriflux Smith Lake 2, 64.8661 °N, −147.8567 °W) is a mature black spruce site with permafrost (Ueyama et al., 2018b, 2014). Details of these sites are found in (Marshall et al., 2019). We also selected field sites within the study landscape for site-scale model evaluation of heterotrophic respiration (NP, 64.8 °N, −147.8667 °W, (Vogel et al., 2005). These sites were dominated by mature black spruce, ranging in age from 75 to 120 years. Details of these sites are found in (Vogel et al., 2005).

2.9. Model inputs

2.9.1. Meteorological and climate data

Meteorological data for our model calibration sites are described in detail in (Marshall et al., 2021a, 2021b). At our recently burned site (US-Rpf), all meteorological variables, including daily air temperature, relative humidity, wind speed, downward shortwave radiation, and precipitation, were available online from on-site meteorological towers (Ueyama et al., 2019, 2018a), except for winter precipitation (Marshall et al., 2021a). To obtain winter precipitation, we used snow depth data from the nearby US-Prr AmeriFlux site and estimated liquid water content of new snow accumulation based on the internal algorithm used in SHAW (Anderson, 1976). Temperature, relative humidity, and wind speed data for our birch-dominated site (UP1A) were available from on-site meteorological towers, though some gap-filling was necessary using nearby weather station data (Marshall et al., 2021a). Downward shortwave radiation was obtained from the US-Uaf AmeriFlux site; precipitation data were obtained from the LTER1 site. Daily air temperature, relative humidity, wind speed, and downward shortwave radiation were obtained from the Geophysical Institute Permafrost Laboratory for the coniferous site (Smith Lake 2). Minimal gap filling was required for air temperature and relative humidity; data from the previous day was used when necessary (Marshall et al., 2021a). In contrast, 27% of the wind data were missing. We filled gaps using linear regressions against co-located wind sensors (at different heights) at the same site for the rest of the missing periods. Daily precipitation data were obtained from the Fairbanks Airport weather station (Menne et al., 2012). Soil moisture (i.e. liquid water content) used for calibration was available at all sites, though depths varied.

DGS requires a full suite of meteorological climate inputs including air temperature, relative humidity, wind speed, downward shortwave radiation, and precipitation at a daily resolution. At the time of this study, downscaled climate data with these characteristics were available for only two GCMs (Global Climate Models) and one RCP (Representative Concentration Pathway). We used dynamically downscaled daily climate data from the NCAR-CCSM4 GCM (Leonawicz et al., 2015) to create our historical and future (RCP 8.5) climate inputs extending from 1970 to 2100 (Supplemental 1). Data were downscaled by the Scenarios Network for Alaska and Arctic Planning (SNAP) using the Weather Research and Forecasting (WRF) model to a 20 km resolution (Bieniek et al., 2016; Lader et al., 2017). Because the climate data were not bias-corrected, we performed a bias-correction step using a quantile mapping approach with the ERA-Interim reanalysis data (downscaled and also provided via SNAP) acting as our observed data (Leonawicz et al., 2015) using the qmap package in R (Gudmundsson and Gudmundsson, 2012).

For the sake of computational efficiency, LANDIS-II uses "climate regions", that are areas of relatively homogenous climate, rather than gridded climate data (Scheller et al., 2007). To determine the optimal number and spatial configuration for the climate regions in our landscape, we performed a spatial k-means cluster analysis using the climate change projections of precipitation and average temperature from 2000 to 2100 aggregated monthly data using the 'cluster' package in R (Maechler et al., 2022). We initially planned to delineate climate regions using monthly PRISM temp and precipitation to find clusters of similar climate areas on our landscape, but we decided that delineating climate regions using the GCM projections would produce climate regions that were more reflective of the spatial configuration of the climate streams and account for future spatial shifts in climate variables. We also found that it was necessary to bias correct temperatures in areas subject to elevational or winter temperature inversion effects at a finer scale than the downscaled GCM (20 km). We did an additional cluster analysis of mean winter temperatures from PRISM 30-year 800-m normals for each climate region (PRISM Climate Group: Oregon State University, 2021), thereby creating subregions. We then compared monthly PRISM temperatures within these subregions to the GCM data for corresponding years and used a delta approach to generate new daily temperature values for each climate region. Because the temperature variables were bias-corrected individually, daily specific humidity was also corrected to ensure that it was not greater than saturated specific humidity at the minimum daily temperature.

For climatic conditions representative of the recent historical period, we calculated daily temperature and precipitation from 1970 to 1990 for each climate region. Climate data for the "historical'' climate scenario were randomly selected, one calendar year at a time, from this 20-year dataset to generate a 50-year timeseries of climate that we could compare to a 50-y climate change projection (Figure S2–1, S2–2). To simulate climate change, we used projected data for 1990–2100, which exhibited an average increase in temperature of 4.7 °C and a change in precipitation of ±264 mm.

2.9.2. Vegetation data

We created four single cell simulations for our field sites for model evaluation. Our recently burned site (US-Rpf) was initialized with 6-year old birch and quaking aspen cohorts (Ueyama et al., 2019, 2018a). Our deciduous site (UP1A) was initialized with 20-year old paper birch and 8-year old aspen (van Cleve et al., 2015a), our coniferous site (Ameriflux Smith Lake 2) was initialized with 78-year old black spruce (Ueyama et al., 2018b, 2014) and our mature coniferous site (NPS) was initialized with 110-year old black spruce (Vogel et al., 2005).

We also created an initial landscape map of species composition, species' age and biomass at a resolution of 4 ha, by imputing USDA Forest Inventory and Analysis (FIA) data (Burrill et al., 2018) onto maps of forest types and stand age with species ages estimated using site index curves (full description of procedures outlined in Supplemental 3). Shrub percent cover by layer from FIA was used to derive cohort biomass values for each plot. This relationship between shrub percent cover and biomass was derived by analyzing data from Bonanza Creek LTER ('Species Percent Cover (1975–2009)' and 'Species Count (1975–2004)), which included stem densities by stem class. Allometric equations for boreal alder and willow (Berner et al., 2015) were used to crosswalk stem classes (BD) within the Bonanza Creek dataset to biomasses and heights for alder and willow. These heights were used to place species in a particular layer category (as defined by FIA), then linear regressions were run between percent shrub cover and biomass for each species by layer and the resulting coefficients were used to assign shrub biomass to each FIA plot in the database. Stand age was used to define shrub cohort ages. Biomass of moss functional types by plot are included in FIA data for the Tanana region so moss functional type cohorts with these biomasses were imputed along with trees and shrubs. We included five tree species, four shrub species, and three moss functional groups in our map, based on species present in the FIA database (Table 1). The most abundant species in our landscape were the mosses, which covered almost 90% of the landscape. The most dominant tree species were white and black spruce, which dominated 52% and 56% of the landscape, respectively, with overlapping distributions. Biomass was dominated by white and black spruce which together comprised 40% of the total landscape biomass. Paper birch contributed about 22% to total biomass at the landscape-scale.

2.9.3. Hydrology and permafrost

Input files for the SHAW and GIPL submodules of DGS were identical for the single-cell and landscape simulations. Each cell was automatically assigned to a THU, which was delineated based on climate zone (1–5), vegetation type (i.e. conifer or hardwood), stand age (i.e. 0–40 y was young, >40 y was considered old), slope (i.e. 0–10, 11–33), and aspect (i.e. north and south aspects). Vegetation characteristics (e.g. biomass, leaf area, and height) for SHAW were calculated using published values and allometric equations for the dominant vegetation, as detailed in (Marshall et al., 2021a). Leaf phenology was derived from snowmelt simulations, based on observed relationships between snow disappearance date and the day of leaf-on (Marshall et al., 2021b). Soil parameters (texture,% organic matter, and bulk density) were based on published values from soil pits (Yarie et al., 1998). Saturated volumetric water content at each soil depth was estimated based on the maximum observed water content at each site. Parameters associated with soil water retention curves and hydraulic conductivity were obtained from the National Cooperative Soil Survey Soil Characterization Database for sites throughout interior Alaska (Beaudette et al., 2021; Burt, 2009). Ground temperature data at the field sites (Ueyama et al., 2018b, 2018a; van Cleve et al., 2015b) were used to calculate thermal properties for live moss, dead moss, and mineral soil layers.

Table 1
Species simulated in this study.

Scientific Names	Common Names
Picea mariana	Black spruce
Picea glauca	White spruce
Betula neoalaskana	Alaska paper birch, resin birch
Populus tremuloides	Quaking aspen
Populus balsamifera	Balsam poplar
Larix laricina	Tamarack
Salix spp.	Willow
Alnus spp.	Alder
Betula nana	Dwarf birch
Sphagnum spp.	Sphagnum peatmoss
Feathermoss functional group includes: *Hylocomium* spp., *Pleurozium* spp., *Thuidium* spp., *Kindbergia* spp., *Brachythecium* spp.	Feathermoss
Turfmoss functional group includes: *Bryum* spp., *Mnium* spp., *Polytrichum* spp.	Turfmoss

2.9.4. Soil carbon

Initial soil characteristics (e.g. initial microbial CN, initial enzyme concentrations) for DAMM-McNiP were derived from (Abramoff et al., 2017), except for C:N ratios of litter, soil, and microbes, bulk density, and particle density which were based on published values in interior Alaska (Vogel et al., 2005). Input maps of soil organic matter, soil texture, soil depth, soil drainage class, field capacity, and wilting point were created using the State Soil Geographic data available from USDA-NRCS for the state of Alaska at a 1:1000,000 scale (Soil Survey Staff, 2020).

2.9.5. Wildfire data

Given its inherent spatial nature, wildfire was only simulated at the landscape scale. Data on ignitions came from the spatial wildfire occurrence data for the US (1992–2015; (Short, 2021). Ignitions were then related to FWI, calculated in the Climate Library of LANDIS-II (Lucash and Scheller, 2021), using the 'zeroinf' function within the 'pscl' package in R (Jackman et al., 2015) to simulate ignitions. To estimate probability of spread, daily fire perimeters from the GeoMac database (GeoMAC, 2019, 2020) were used to identify successful or unsuccessful cell-to-cell spread occurrences from historical fires. Daily FWI, daily effective wind speed (calculated from modeled wind speed and derived direction of fire spread), slope and aspect derived from a Digital Elevation model (USGS, 2020a), and relative fine fuels (USGS, 2020b) were then extracted from these cell locations and used as predictors to fit a logistic model of probability of spread. Maximum allowable daily spread was determined by parameters derived from fitting a generalized linear model of maximum daily spread areas derived from the GeoMac database (GeoMAC, 2019, 2020) to associated FWI and effective wind speed.

Model calibration and validation

To calibrate growth in DGS, we conducted single-cell simulations (non-spatial monocultures) with each of our four functional groups (e.g. hardwoods, conifers, shrubs, mosses) comparing the biomass trajectories over time in LANDIS-II with FIA data (Burrill et al., 2018) that have estimates of biomass as a function of stand age (more details in Supplemental 3). We adjusted two parameters (e.g. KLAI, which determines the relationship between LAI and biomass, and the competition index, which affects the competitive ability of different functional groups) to mimic the initial maximum growth rates observed in FIA and used the mortality shape parameter to mimic the longevity-related declines in growth. We also calibrated foliar to wood biomass ratios and above: belowground biomass by comparing the output from these single-cell simulations with FIA data. The proportion of fine and coarse roots was calibrated using literature values of the% of root mass that is devoted to fine roots (36%, (Noguchi et al., 2012). Input parameters that influenced growth were identical between the single-cell and landscape simulations.

To validate landscape-level biomass at the start of the simulation, we compared our tree biomass map of the landscape at time=0 with a global biomass map from GlobBiomass (Santoro, 2018). Our simulated biomass tended to be underestimated within areas that had burned since the year 2000, while areas where biomass was overestimated primarily fell outside of these more recently burned areas. There were fewer FIA plots present within burn scars to use in our imputation of landscape tree composition and biomass, and those data availability limits likely contributed to some of the disagreement within these fire scars. Overall, discrepancies within and outside of the burn scars area also likely due to differences in the source years for the datasets. GlobBiomass was created for the year 2010, while the landcover map and FIA used data from 2017 to 2016, respectively.

To calibrate and validate soil moisture and temperature, we compared simulated and observed patterns of soil moisture and soil temperature at our three of our field sites (Ueyama et al., 2018b, 2018a; van Cleve et al., 2015a). A Bayesian parameter estimation and uncertainty analysis was used to identify appropriate model parameters from a range that was defined through literature review and analysis of available data; this method is fully described in Marshall et al. (2021a). Parameters in GIPL related to snowpack, such as the viscous compaction coefficient, were estimated by maximizing the fit between the observed snow depth to the modeling results across the three field sites.

To calibrate soil respiration, we compared simulated and observed patterns of heterotrophic soil respiration at a field site near Fairbanks, Alaska (Vogel et al., 2005). All input parameters in DAMM-MCNiP were fit by minimizing the residuals of the model using a Newton-type method (function modFit, method Newton, package FME (Soetaert and Petzoldt, 2010) fully described in Abramoff et al. (2017).

To calibrate wildfire ignitions, we ran simulations at the landscape-scale and adjusted the fire ignition intercept until it recreated the observed annual number of fires from 1970 to 1990 (Supplemental 4, Fig. S4–1). We also validated fire spread by comparing the fire size distribution and fire return interval to observations for the 1980–1990 period.

2.10. Experimental design

Single-cell simulations of three field sites were initialized with current vegetation and run for 9–16 years, depending on the available field data using DGS. Model performance was assessed in R (version 1.4.1106) by computing RSME for the model predictions and the observed field measurements of soil temperature and moisture. We also ran single-cell simulations of three field sites with NECN, the predecessor of DGS, and compared the output between the two model extensions and observed field measurements. NECN uses a one-layer approach to simulating soil temperature and moisture so NECN output was compared to the one-layer output from DGS. These simulated values were compared to mean soil temperature and moisture down to maximum soil depth at each of the field sites.

Landscape-scale simulations were run on a 4-ha grid over 50 years (1990–2060 both inclusive) across >397,860 hectares in interior Alaska. We compared wildfire, soil temperature, soil moisture, aboveground biomass, forest type, and species composition under two climate scenarios. The historical climate scenario represented the climate from 1970 to 1990, while the climate change scenario used projections from 1990 to 2040, which exhibited an average increase in temperature of 4.7 °C and precipitation of 264 mm over the historical conditions. All scenarios were replicated five times at the landscape-scale to account for stochasticity from successional dynamics, seed dispersal, regeneration, and wildfire (total of 10 model runs: 2 climate × 5 replicates). Differences in ignitions, area burned, soil temperature, soil moisture and biomass between climate scenarios were compared using Welch's *t*-test with unequal variance. Significance was assessed at a 95% confidence level and p-values less than 0.05 suggested that there was strong support for a difference between scenarios. All data processing and statistical analyses were performed using R (R Core Team, 2022).

To test the effects of soil moisture, soil temperature, and available soil nitrogen on aboveground biomass, we ran four simulations (with 5 replicates each) where we modified the internal code to prevent each factor from affecting growth under climate change. We also ran a simulation without wildfire. We calculated the relative differences in aboveground biomass among these scenarios and our climate change scenario. All data processing and statistical analyses were performed using R. To test the effects of soil moisture and soil temperature on regeneration, we ran two simulations (with 5 replicates each) where we modified the internal code to prevent each factor from affecting regeneration under climate change. We calculated the relative differences in aboveground biomass among these scenarios and our climate change scenario.

3. Results

3.1. Model performance at field sites

Modeled soil temperature generally reproduced the interannual variability and differences between depths in the empirical data at three field sites (Fig. 3). Model agreement between simulated and observed soil temperature based on RMSE, was higher at the coniferous site (Smith Lake 2, 0.3 – 1.7 °C) than the recently-burned (US-Rpf, 1.9 – 2.9 °C) and deciduous sites (UP1A, 1.1 – 2.5 °C). At the burned site, model performance was good, except for the winter of 2013 when it overestimated soil temperature at both 10 cm and 90 cm. At the deciduous site, the model captured the magnitude of soil temperature observed at the site, though it tended to predict spring warming later than observed at the 0.5 m depth. The model captured summer temperatures extremely well at the conifer site but it simulated lower temperatures than observed at the surface (10 cm depth).

Modeled liquid soil water content generally reproduced the interannual variability and differences between depths in the empirical data at all three field sites (Fig. 4). The RMSE suggests some differences between performance at the sites with higher agreement at the recently-burned (US-Rpf, 0.03 m^3 m^{-3}) and deciduous (UP1A, 0.01–0.04 m^3 m^{-3}) sites than the coniferous site (Smith Lake 2) with a RMSE of 0.02–0.07 m^3 m^{-3}. The DGS extension captured spring wetting due to snowmelt and summer rainfall events quite well at all three sites. However, simulated soil moisture was overestimated in the winter at the burned site, though it tracked the timing and magnitude of soil moisture in the summer. At the deciduous site, DGS underestimated soil moisture in the top 10–20 cm, though it captured the timing and magnitude of spring snowmelt that was observed at the field site. Performance was better at lower depths; there was higher agreement at 0.5 m (RMSE= 0.01 m^3 m^{-3}) than 0.2 m (RMSE = 0.04 m^3 m^{-3}) or 10 cm (RMSE = 0.02 m^3 m^{-3}). At the coniferous site, simulated soil moisture was similar to observed values at 10 and 40 cm, but the simulated timing of spring thaw in the active layer was earlier than observed. DGS did not capture the seasonal variation observed at 85 cm depth.

Modeled soil respiration generally reproduced the seasonal variation in the empirical data at the field site (Fig. 5), but greatly underestimated respiration in the summer months. Percent differences were much smaller in June (16%) than July (39%) and August (61%) between modelled and empirical estimates. The high RMSE (18 g C m^{-2}) reflects these differences and suggests that additional calibration may be necessary to confidently simulate soil respiration using DGS.

When compared to the original succession extension of LANDIS-II, DGS performed better than its predecessor, NECN. The original succession extension of LANDIS-II, NECN, produced annual mean soil temperatures that were similar to observed values, but NECN consistently overestimated the seasonality of soil temperature at all three field sites. NECN simulated a 49.5 °C difference in minimum and maximum monthly soil temperature influencing tree growth, but the observed variation across the field sites was only 19.8 °C (Fig. 6). DGS simulated a 21.7 °C difference in minimum and maximum monthly soil temperature, only 10% higher than the observed range. Across all sites, NECN overestimated soil temperature in the summer months, simulating a mean summer temperature of 15.5 °C, compared to the mean of 5.3 °C by DGS and the observed value of 5.4 °C. NECN underestimated soil temperature in the winter months, suggesting it was 11 °C colder than the observed monthly mean of −2.2 °C. DGS simulated winter temperatures that were within 1 °C of the observations. The improved simulation of soil temperature by DGS was particularly notable in the spruce site. Observed soil temperature ranged from −0.4 °C to 2.6 °C; simulated soil temperature in NECN ranged from an average of −16.2 °C in the winter to 15.2 °C in the summer, whereas soil temperature in DGS ranged from an average of −2.6 °C in the winter to 4.1 °C in the summer.

DGS simulated soil moisture influencing tree growth better than its predecessor (Fig. 6). NECN simulated soil moisture that was 86% lower than the observed values across all field sites, while DGS simulated values within 21%. Simulated annual mean soil moisture was only 0.03 m^3 m^{-3} in NECN, whereas DGS simulated a mean of 0.16 m^3 m^{-3} that was within 21% of the observed mean of 0.20 m^3 m^{-3} across all field

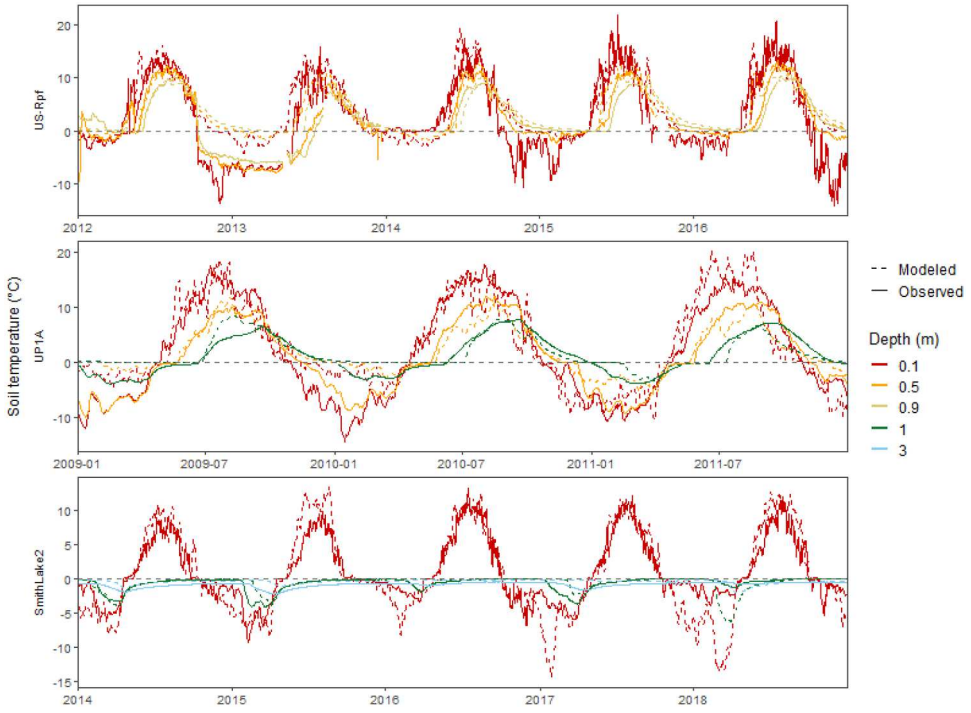

Fig. 3. Time series plots of modelled and observed monthly soil temperature at our three calibration sites. US-Rpf (recently burned and dominated by paper birch), UP1A (paper birch dominated), and Smith Lake 2 (spruce-dominated) show distinct seasonal patterns with soil temperature highest in the summer months. Soil temperature was simulated at 54–58 depths throughout the soil profile down to 75 m, but only the depths for which there is empirical data are shown here.

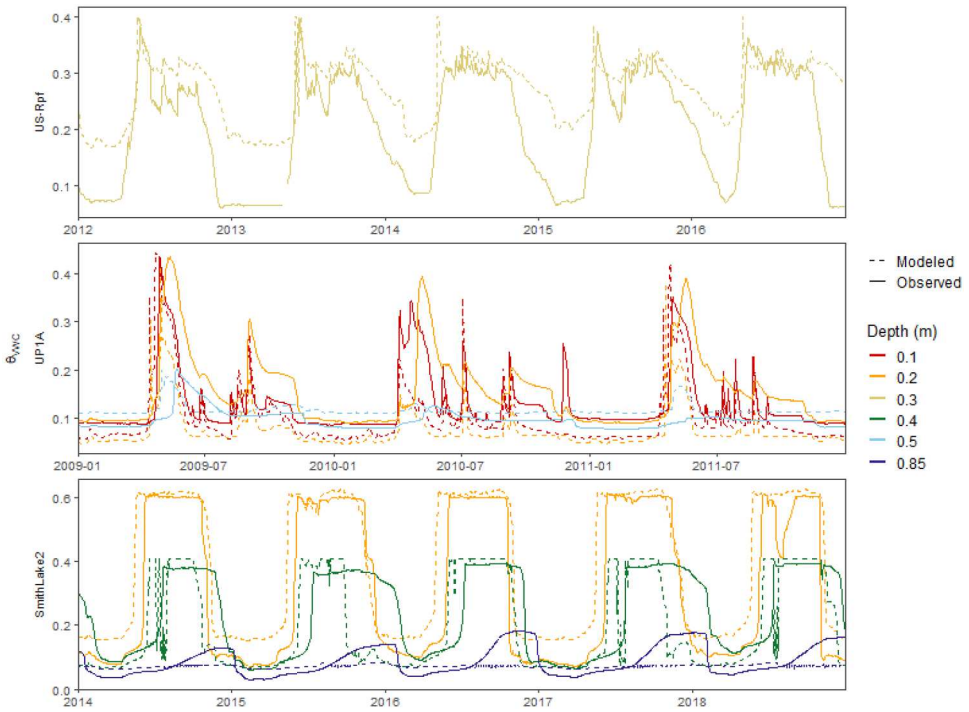

Fig. 4. Time series plots of modelled and observed monthly liquid soil moisture at our three calibration sites. US-Rpf (recently burned and dominated by paper birch), UP1A (paper birch dominated), and Smith Lake 2 (spruce-dominated) show distinct seasonal patterns with soil moisture highest in the summer months. Soil moisture was simulated at 18–22 depths throughout the soil profile down to 6 m, but only the depths for which there is empirical data are shown here.

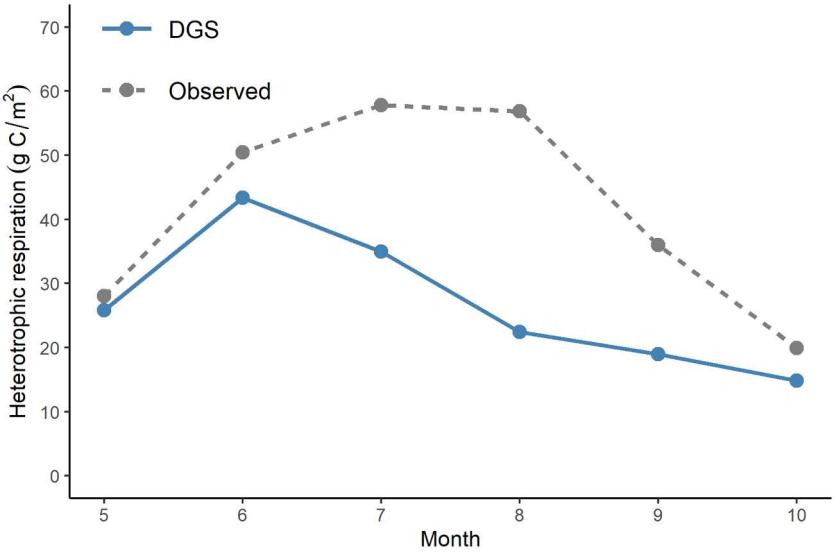

Fig. 5. Time series plots of modelled and observed monthly heterotrophic respiration at a mature black spruce stand. DGS simulates soil respiration throughout the year, including winter months, but only the months for which there is empirical data are shown here.

sites. In the summer months, when moisture is influencing tree growth, DGS outperformed NECN at the recently-burned and coniferous sites, but not at the deciduous site. At the burned site, DGS simulated soil moisture that was 26% lower than observations in the summer, whereas NECN simulated values that were 89% lower. Available soil moisture in DGS ranged from 0.17 in the winter to 0.2 $m^3\ m^{-3}$ in the summer in the burned site, while observed values ranged from 0.07 (winter) to 0.29 $m^3\ m^{-3}$ (summer). Soil moisture in NECN ranged from 0.008 in the winter to 0.03 $m^3\ m^{-3}$ in the summer. At the birch site, NECN performed better than DGS in the summer. NECN simulated soil moisture that was only 12% lower than observations in the summer, whereas DGS simulated values that were 65% higher. Simulated summer soil moisture in NECN (0.09 $m^3\ m^{-3}$ in DGS) was similar to observed values in the summer (0.1 $m^3\ m^{-3}$), but DGS simulated values much higher (0.17 $m^3\ m^{-3}$). At the spruce site, DGS outperformed NECN in the summer, simulating soil moisture that was higher in agreement with observed values. At the spruce site, soil moisture in NECN ranged from 0.02 in the winter to 0.07 $m^3\ m^{-3}$ in the summer. DGS simulated 0.07 $m^3\ m^{-3}$ in the winter and 0.23 $m^3\ m^{-3}$ in the summer, while observed values ranged only from 0.18 (winter) to 0.40 $m^3\ m^{-3}$ (summer). Overall model performance by DGS was not explicitly computed in these comparisons with NECN, because NECN only simulates surficial soil temperature and

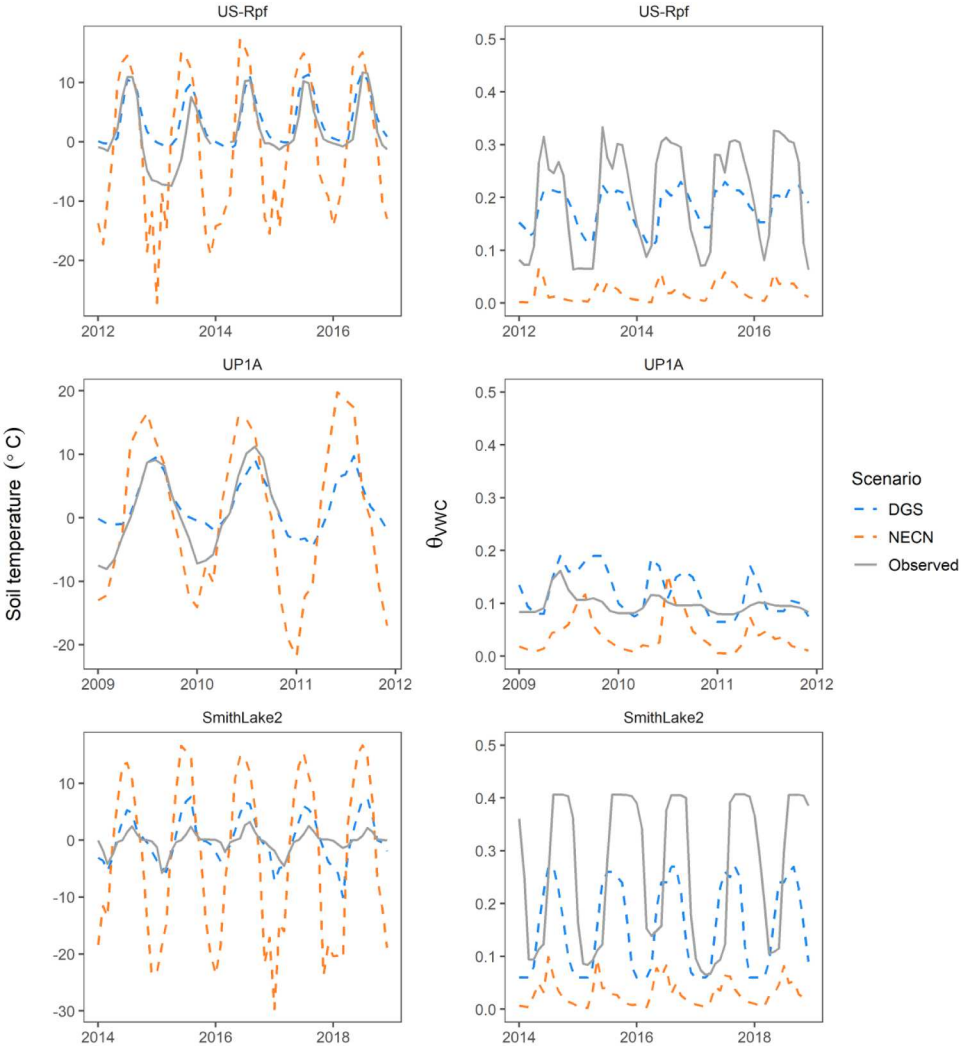

Fig. 6. Time series plots of monthly soil temperature and liquid soil moisture measured in the field and modelled by DGS and NECN at US-Rpf (recently burned and dominated by paper birch), UP1A (paper birch dominated), and Smith Lake 2 (spruce-dominated). NECN uses a one-layer approach to simulating soil temperature and moisture so we compared NECN output to comparable (one-layer) output from DGS and observed mean values down to maximum soil depth for each site (201 cm for US-Rpf; 77 cm for UP1A and Smith Lake 2). The fit between DGS and observations is much lower here than in Figs. 3 and 4 when comparisons are made between similar depths.

available soil moisture. Instead of comparing soil temperature and moisture at similar depths (as in the previous analysis), we were forced to compare simulated average soil moisture (average soil moisture down to rooting depth) with observed soil moisture at one depth (rooting depth), which results in artificially low RSME values.

3.2. Model results at the landscape-scale

After model calibration with data from the field stations, the DGS extension was run at the landscape-scale with wildfire to explore how climate change (i.e. NCAR-CCSM4 RCP 8.5) may affect wildfire, soil moisture, soil temperature, and vegetation.

As expected, climate change had a significant impact on wildfire. The number of wildfire ignitions was significantly higher under climate change than historical climate across the entire simulation period ($p \leq 0.01$), but the differences between climate scenarios also became more pronounced over time (Fig. 7). By mid-century, the number of mean annual ignitions across the landscape was 1.8 under historical climate and 2.8 under climate change. The variability in ignition rates was also significantly different between climate scenarios (Levene's test, $p \leq 0.004$) with 37% higher variation under climate change (variance = 0.78) than historical climate (0.49). Annual area burned increased over time and was significantly higher under climate change (3326 ha) than historical climate (1687 ha, $p \leq 0.001$). The number of fire years with over 10,000 hectares burned was only two under historical climate, but seven under climate change.

At the landscape-scale, there was significantly less subsurface permafrost, quantified using soil temperature at 3 m, under climate change ($p \leq 0.0001$). Over the course of the simulation, soil temperature increased slightly under historical climate (by 0.16 °C) but increased dramatically under climate change by 1.1 °C (Fig. 8). Across the 50-y simulation period, soil temperature was significantly higher under climate change than historical climate for all forest types, but the rate of change differed by forest type. Soil temperature increased at a much faster rate in the hardwoods than the conifers under climate change. In the conifer sites, soil temperature increased by 0.007 °C per year under climate change. In the young and mature hardwoods, soil temperature increased by 0.03 °C and 0.39 °C per year, respectively, resulting in a 1.9 °C and 1.5 °C change by mid-century. Variation in soil temperature was higher under climate change (Levene's test, $p \leq 1 \times 10^{-9}$) driven by the stochasticity of wildfires.

Annual simulated tree-available soil moisture at the landscape-scale was highly variable but was relatively similar ($p < 0.04$) between the historical and projected climate change scenarios, despite higher precipitation under climate change (Fig. 9). During one period from 2015 to 2022, soil moisture was 14% higher under climate change, but this was due, at least in part, to precipitation which was 29% higher during that period. Soil moisture declined over time, with a 10% decline under historical climate and 27% under climate change by mid-century. Variability was higher under historical climate (Levene's test, $p \leq 0.000000001$), but that was primarily because different climate streams were used in each replicate. Climate change had the strongest effect on

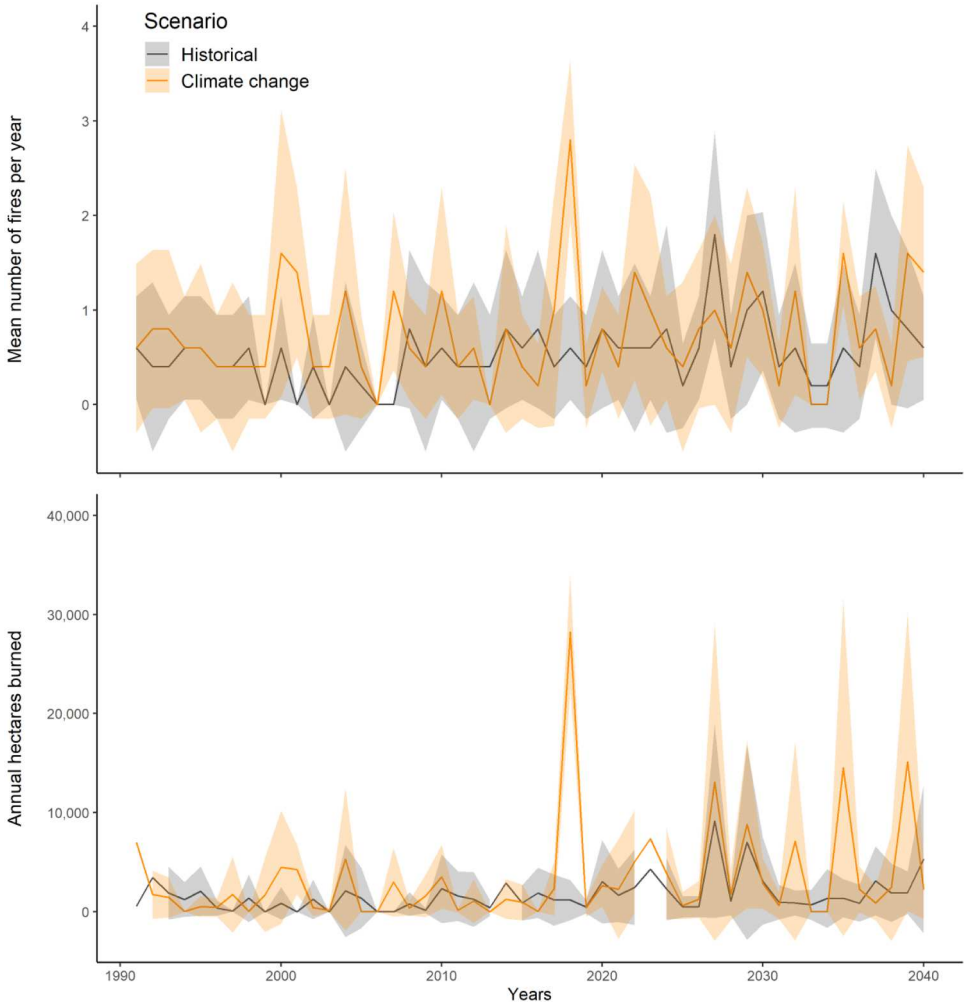

Fig. 7. Landscape-level annual ignitions (top) and hectares burned (bottom) under two climate scenarios through 2040. Ribbons represent the standard deviation.

soil moisture at sites dominated by young conifers (Welch's test, F-value 471.7, $p \leq 10^{-9}$), which was expected because soil moisture has a strong effect on post-fire regeneration in the model. Available soil moisture was higher in the conifer-dominated sites than in the sites with deciduous species under both of the climate scenarios.

Simulated mean aboveground biomass density was significantly affected by climate change (Welch's *t*-test with unequal variance, $p \leq 0.00002$). Under historical climate, aboveground biomass initially increased by 30%, but then stabilized around 2010 (Fig. 10). Under climate change, biomass also increased (27%) until 2010, but later declined by 55% under climate change by 2050. Annual variation at the landscape-scale was relatively small, with some fluctuations due to wildfire and successional dynamics. Most of the variation in aboveground biomass under climate change was due to soil moisture (~53%) until 2018 when fire became the dominant driver, explaining 70% of the variation (Fig. 11). Soil moisture was the main limitation to regeneration under climate change. Soil moisture explained ~80% of the variation in biomass of regenerating trees and shrubs under climate change, and became more important over time, explaining over 90% of the variation by 2040.

The dominant forest type shifted during the simulation; the percentage of the landscape dominated by conifers declined from 71% to 54% under historical climate, but under climate change conifers only dominated 52% of the landscape by the year 2040 (Fig. 12). Under historical climate, most species that were initially high in biomass and abundance remained so until the end of the simulation, including black spruce, white spruce, and paper birch (Fig. 13). Alder, shrub birch, and willow increased their landscape-level biomass over time, though their extent remained constant. Under climate change, however, white and black spruce decreased dramatically in biomass by 69% and 50%, respectively even while their extent remained constant. Paper birch also had lower biomass under climate change, but the other hardwoods remained relatively unaffected by climate change.

Soil C increased annually by only 0.26%, with a slightly higher rate under climate change (0.28%) than historical climate (0.24%, Fig. 14). Over the 50-year simulation period, DGS simulated an average gain of 4.9 Tg ± 0.13 Tg (SD) of C under historical climate and 5.6 Tg ± 0.05 Tg (SD) of C under climate change across the entire landscape.

4. Discussion

4.1. Model evaluation

DGS captured the variation in soil temperature across depths, seasons, and water years reasonably well, though the model tended to simulate surficial temperature (10 cm depth) much warmer than observed at the spruce site. This suggests that the model was unable to capture the ability of the surface litter layer to moderate surface temperatures in alignment with other studies that have highlighted the challenges of simulating frozen soil thermal conductivity (He et al., 2021). Mosses and associated soil organic horizons have low thermal conductivity values relative to mineral soil (Farouki, 1981) and therefore reduce vertical heat fluxes through the soil profile and insulate soil from warm air temperatures. These errors may also originate from

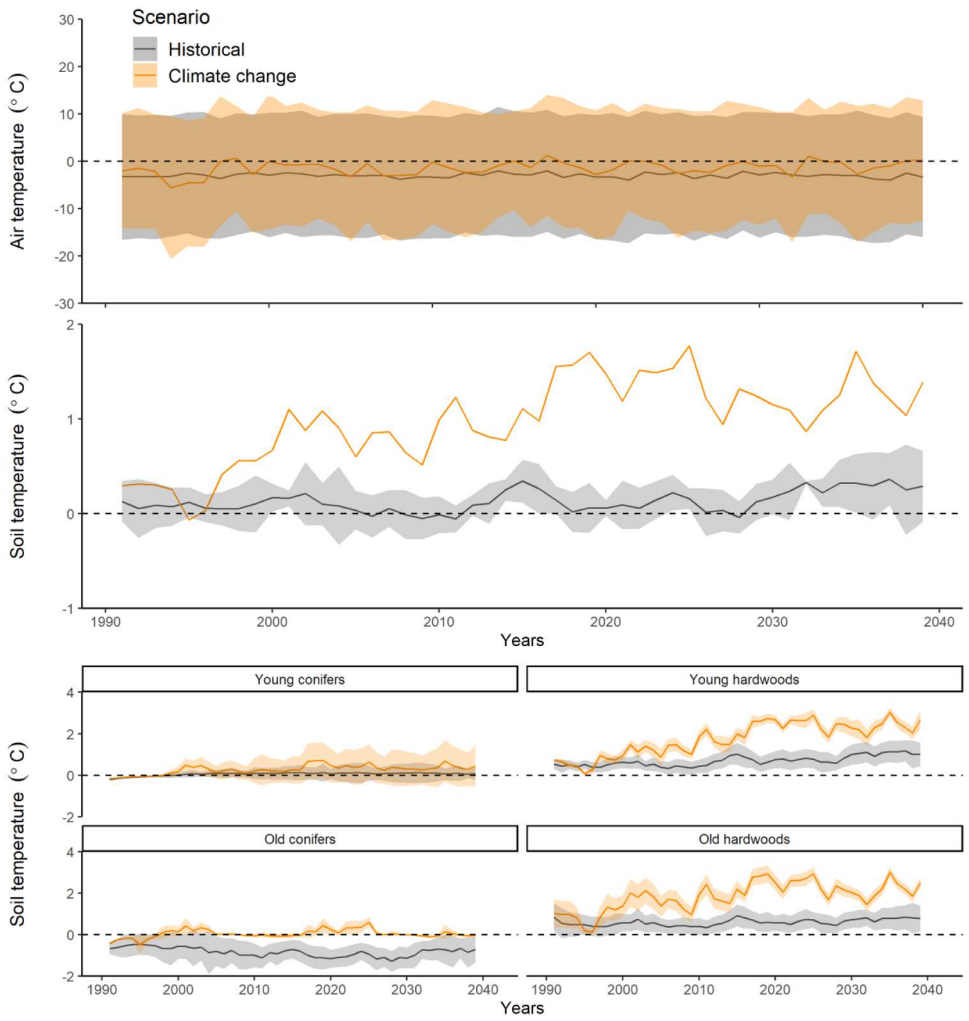

Fig. 8. Time series plots of annual air temperature (top) and soil temperature at 3 m (i.e. standard depth to characterize near-surface permafrost) averaged across the entire study area (middle) and by vegetation type and age (bottom) for two climate scenarios. Young hardwoods and conifers range in age from 0 to 40 years old; old hardwoods and conifers range from 40 to 500 years old. Ribbons represent the standard deviation.

advective heat fluxes associated with lateral water transport not simulated by the model; for that reason, the model results – particularly those pertaining to soil moisture and temperature – are most reliable in upland areas that have less net lateral flows than lowland sites within the spatial domain. Despite the poor agreement at the surface layer at the spruce site, DGS captured the temperature dynamics well at deeper depths and at other sites, indicating that the model effectively simulates important controls on soil temperature and the thermal status of permafrost in high-latitude ecosystems (Bonan and Shugart, 1989; Dyrness, 1982; Nicolsky et al., 2007; Yoshikawa and Hinzman, 2003).

Across all field sites, DGS generally captured the variation in soil moisture across depths, seasons, and water years reasonably well, though there were some discrepancies at each site. Soil moisture was overestimated in the summer months at the birch site, likely caused by underestimating evapotranspiration ((Marshall et al., 2021b). Transpiration comprises a large fraction of evapotranspiration (Jasechko et al., 2013), but is not well understood in boreal regions, despite its importance to vegetation dynamics and regional climate. Most landscape and Earth System Models do not simulate the lateral transfer of water that can influence evapotranspiration and therefore cannot capture increased lateral leaching with storm events nor the ability of laterally-transported groundwater to sustain evapotranspiration during summer drought. This is also the case in DGS but should be a target area for future model development to advance the understanding of lowland areas, common in interior Alaska and throughout boreal forests. At the burned site, simulated soil moisture tracked observed values in the summer, but overestimated values in the winter when errors in simulated snow depth or density might cause disparities. Without snow data at this site or a nearby site with similar vegetation conditions and fire history, it is difficult to identify the specific mechanisms that produce the discrepancy and emphasize the need for more intensively monitored stands in the boreal regions.

Overall, DGS led to a more realistic simulation of soil temperature and moisture than its predecessor, NECN at the three field sites. NECN consistently overestimated the seasonal fluctuations of soil temperature (Fig. 6), leading to the conclusion that the mature spruce site lacked permafrost, despite field observations that showed otherwise. Also, NECN simulated very low soil moisture at all field sites, suggesting that water limitation was more severe at all the sites throughout the year than field observations suggest. With the integration of a physically-based energy and water budget model (SHAW) and permafrost model (GIPL) into the succession model, DGS produced a much higher correlation with observed soil temperature and moisture across all sites and, most importantly, was able to reproduce the permafrost conditions at the spruce site.

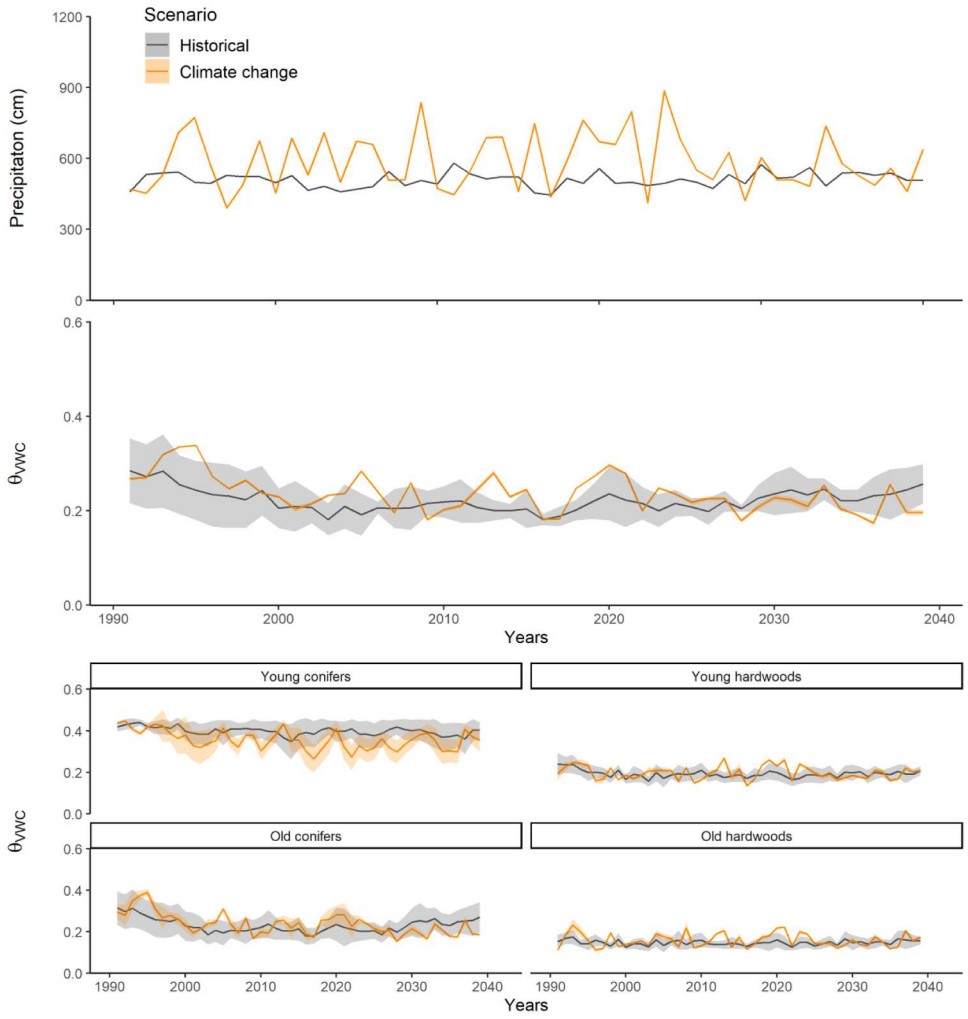

Fig. 9. Time series plots of annual precipitation (top) and modelled liquid soil moisture (integrated from 0 to 50 cm) averaged across the study landscape (middle) and by vegetation type and age (bottom) for two climate scenarios. Young hardwoods and conifers range in age from 0 to 40 years old; old hardwoods and conifers range from 40 to 500 years old. Ribbons represent the standard deviation.

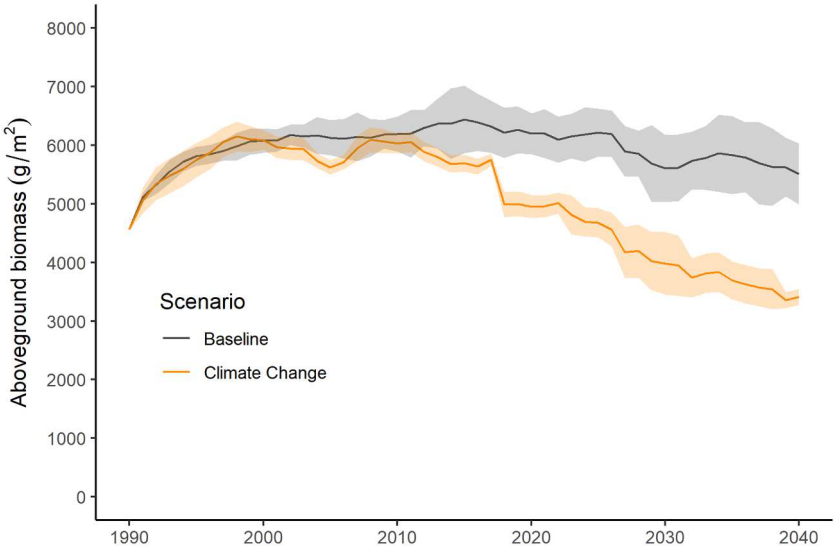

Fig. 10. Changes in aboveground biomass density (g biomass m^{-2}) (top) through time in the study landscape under two climate scenarios. Ribbons represent the standard deviation.

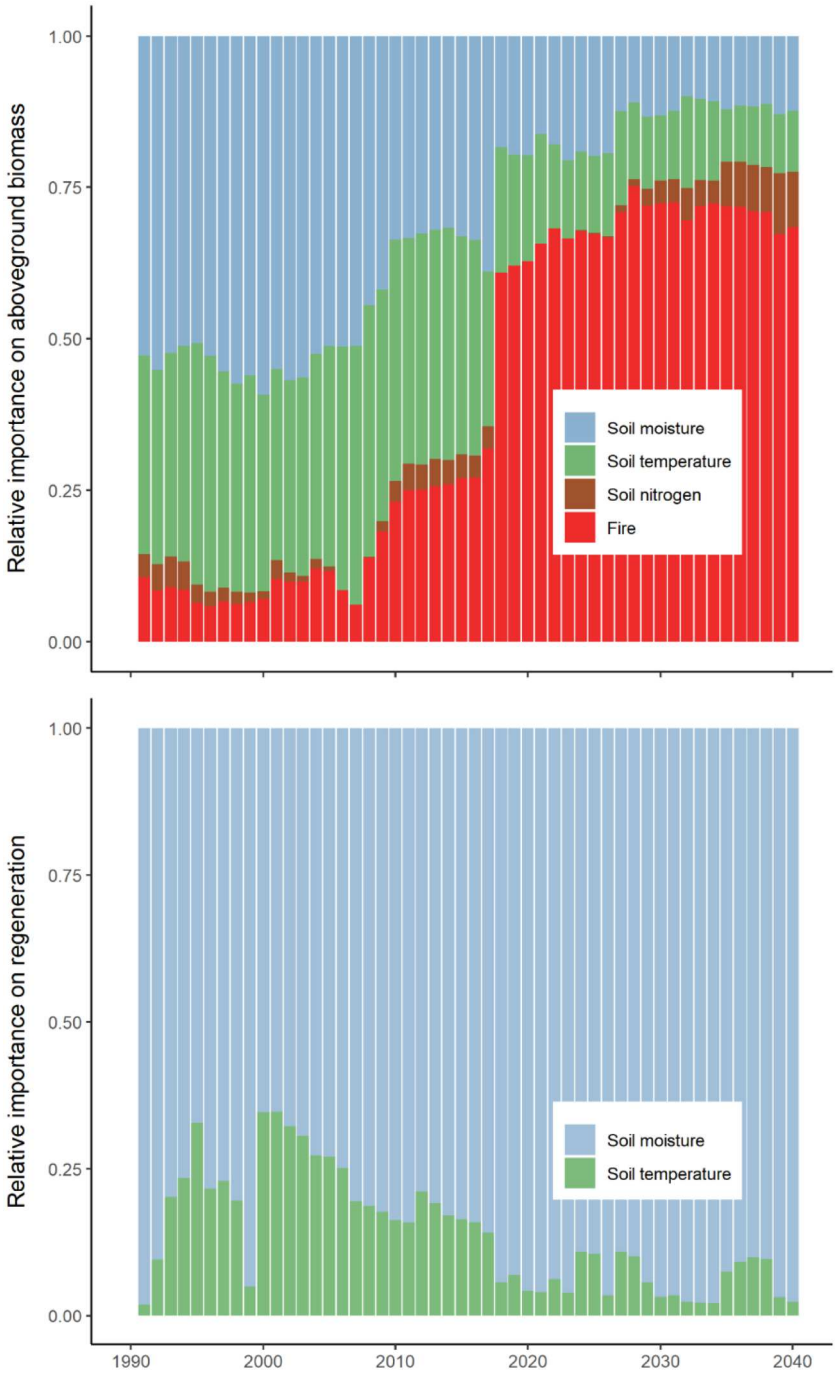

Fig. 11. Changes in the relative importance of the main factors influencing aboveground biomass (soil moisture, soil temperature, soil nitrogen, and fire) and regeneration (soil moisture and temperature) through time in the study landscape under climate change.

4.2. Wildfire and soil dynamics under climate change

Over the last several decades, Alaska has witnessed an increase in area burned (Calef et al., 2015; Kasischke et al., 2010; Kasischke and Turetsky, 2006) and the number of years with large fires (Kasischke and Turetsky, 2006), which our landscape-scale simulations suggest will continue to increase as the climate warms. Under climate change, DGS simulated a 65% increase in area burned in comparison with historical climate, which is more than double the 14–30% projected area based on previous studies (Bachelet et al., 2005; M. Flannigan et al., 2009). However, the results agree well with Flannigan et al. (2009) who projected a 50% increase in area burned in Canada under climate change.

As expected, soil temperature at the landscape-scale was affected by both climate and vegetation type. Interior Alaska is located within the discontinuous zone of permafrost (Jorgenson et al., 2010), and soil temperature is driven by complex feedbacks between climate (Jorgenson et al., 2010), fire (Minsley et al., 2016), and vegetation (Jorgenson et al., 2001). As air temperature warms under climate change, soil temperature and active layer thickness increases and the depth to permafrost increases. However, changes in vegetation type, soil moisture, and the insulative properties of snow also play an integral role in maintaining permafrost integrity by buffering changes in air temperature (Jorgenson et al., 2010). Coniferous forests with their dense canopies and thick organic horizons buffer the effects of warmer temperatures, acting as a thermal insulator between the atmosphere and the ground (Walker et al., 2003). Our model captures these dynamics

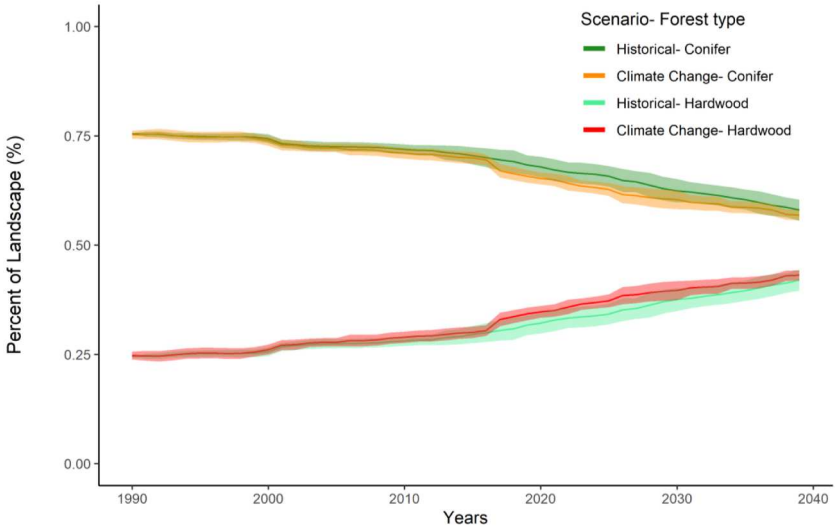

Fig. 12. Changes in percent area of the dominant forest type through time in the study landscape under two climate scenarios. Ribbons represent the standard deviation.

Fig. 13. Change in aboveground biomass density (g biomass m^{-2}) of each species through time under two climate scenarios.

with soil temperature increasing by 0.02 °C/y in conifers and 0.07 °C/y in hardwoods under climate change. Overall, our rates of near-surface (3 m) soil warming (0.019 °C/y) under climate change are similar to observed estimates in interior Alaska (~0.01–0.037 °C/y, (Clow, 2008; Romanovsky et al., 2019), Southern Norway (0.015–0.095 °C /year, (Isaksen et al., 2011), Siberia (0.01–0.08 °C/y, (Malkova, 2010; Oberman, 2008; Vasiliev et al., 2008), and Mongolia (0.015 °C/year, (Sharkhuu et al., 2007). All Earth System Models project near-surface permafrost degradation over large geographic areas of the boreal and arctic ecosystems, though the extent and rate of change differs between models (Koven et al., 2013; McGuire et al., 2018).

The simulation results here demonstrate that vegetation type had a greater effect on soil moisture than climate change at the landscape scale (Fig. 9), given the large differences in soil moisture between hardwoods and conifers. Forest type influences soil moisture via depth to permafrost, differential transpiration rates among species, interception and throughfall of snow and liquid precipitation, forest impacts on the surface energy balance, and different organic matter accumulation patterns. Hardwoods often have lower interception rates and greater throughfall but higher stomatal conductance and transpiration than

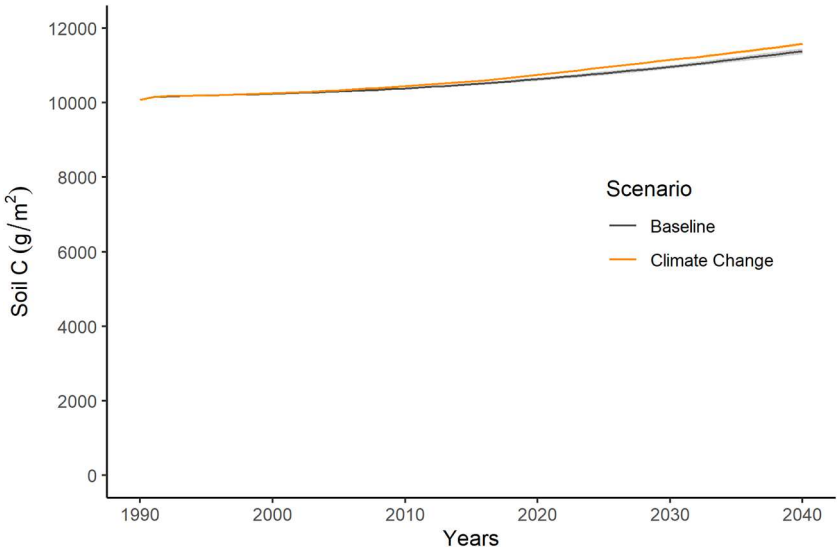

Fig. 14. Change in soil organic C (g C m $^{-2}$) through time under two climate scenarios.

conifers (e.g., (Cable et al., 2014), which often collectively results in lower soil moisture under hardwood canopies, as simulated in this study. Given these hardwood forest types are projected to become increasingly prevalent as wildfire frequency increases (Hansen et al., 2021; Johnstone et al., 2010b; Mann et al., 2012), this could have ramifications for streamflow and overall productivity across the landscape (Barichivich et al., 2014). Although precipitation increased under climate change (Bieniek et al., 2014; Lader et al., 2017), there was high uncertainty associated with these trends (Meredith et al., 2019) and it did not cause a net increase in soil moisture in our study. The magnitude of projected changes in soil moisture in Arctic regions varies widely with most studies showing a decline in soil moisture, primarily due to deep drainage following permafrost thaw, though a few studies project wetting trends (Andresen et al., 2020). The IPCC denotes soil moisture as a major source of uncertainty in this region (Meredith et al., 2019), given the complex interactions and feedbacks between increasing precipitation, longer and warming growing seasons causing greater evapotranspiration, shifts in vegetation type, and increases in fire frequency.

Given that DGS underestimated C lost as soil respiration, soil C is likely overestimated with DGS, though the projections of soil carbon over time generally agree with other studies showing relatively stable pools for the next 50 years. Interior Alaska is not expected to show substantial declines in soil C until after 2050 (McGuire et al., 2018), when this region is projected to be a net source of soil C to the atmosphere (Koven et al., 2011). Losses in soil carbon associated with higher soil temperatures in boreal forests have been documented across numerous field studies (Eliasson et al., 2005; Melillo et al., 2017; Shabaga et al., 2022) and some modeling studies (H Genet et al., 2013), but these studies are focused primarily on organic horizons, which are only a small fraction of the total soil C pool. Model projections of soil C under climate change remain highly uncertain with the full range of possibilities including models that predict gains in soil C (ORCHb), constant soil C (TEM6), gains and then losses starting in 2150 (UVic), and constant soil c followed by losses starting in 2100 (CLM 4.5; SiBCASA; (McGuire et al., 2018). The short duration of our modeling study and makes it challenging to project how climate change will affect soil C, especially given the diverse physical, chemical, and biological factors that influence its stability.

4.3. Aboveground biomass dynamics under climate change

The biomass declines we projected under climate change differ from most other modeling studies in this region. Most models project an increase in aboveground biomass under climate change due to CO_2 fertilization and/or an increase in the length of the growing season (Euskirchen et al., 2017; McGuire et al., 2018; Zha and Zhuang, 2021). The state-and-transition model ALFRESCO-TEM predicted increases in vegetation biomass, both when vegetation was constant or allowed to shift over time (Euskirchen et al., 2016a). Also, the mean increase in vegetation C stocks differed between their climate scenarios with the highest projected C accumulation occurring in response to the fertilization effect of rising atmospheric CO_2 (Euskirchen et al., 2016a). In a recent multi-model approach with eight ESMs, the sensitivities of model NPP responses to climate change were between 1.9% and 15.4%, consistent with the mean of 13% in free-air exchange CO_2 enrichment (FACE) experiments at the time the models were parameterized (Piao et al., 2013). However, this global mean of 13% represents FACE experiments primarily conducted in young, temperate forests with high nutrient availability and not boreal forests (Walker et al., 2021). In the boreal forests of Ontario, Canada, the synergistic effects of rising CO_2 and temperatures increased water-use-efficiency of black spruce by 53% over the past century, but this did not always translate into commensurate increases in growth (Silva et al., 2010). In northern latitudes (51°N), growth (i.e. basal area increment) increased between 1950 and 2007, but growth declined starting in 2000 at mid-latitudes (47–49°N) and 1980 at lower latitudes (45°N). Finally, existing models which do simulate a CO_2 fertilization effect tend to overestimate biomass (Albani et al., 2006), though recent integrations of observations and models have reduced this uncertainty considerably (Keenan et al., 2021). Therefore, without convincing evidence for the potential CO_2 fertilization effect on tree growth in boreal forests, we decided to omit this potential driver of vegetation dynamics though we note this could be an important area for future model development.

Although the simulated biomass trends do not agree with most other modeling studies, our results are consistent with the browning trends observed from remotely-sensed data in the forests of interior Alaska and results with UVAFME. Between 1981 and 2012, gross photosynthesis declined in interior Alaska, while growing season length remained constant in interior Alaska despite rising CO_2 and temperatures (Goetz et al., 2005; Ju and Masek, 2016). This mechanism for this apparent decoupling of growth, CO_2, and warming in forest areas is unknown, but was likely caused by drought stress (Barber et al., 2004; Dai et al., 2004), nutrient limitation (Hobbie et al., 2002), insect and disease damage (Ayres and Lombardero, 2000), and/or changes in resource allocation (Gower et al., 2001). Our projected declines in total aboveground biomass were also aligned with the UVAFME model projections (Foster

et al., 2022). Simulations with UVAFME showed a 24% decline in aboveground biomass under both RCP 4.5 and 8.5 climate emissions scenarios by the end of the century in interior Alaska, though the differences in biomass projections between climate change and historical climate scenarios was relatively small . Our simulations project a comparable 22% reduction in biomass under climate change by mid-century. Our difference in biomass between historical climate and climate change scenarios (1.5 tC ha^{-1}) was similar initially to Foster et al., 2022 (Fig. 10, 2.5 tC ha^{-1}), but by mid-century our difference was 21 tC ha^{-1} while Foster was only 5 tC ha^{-1}. Biomass declines in our simulations resulted from reductions in spruce biomass, with soil moisture and wildfire as the most important drivers. Declines in conifer biomass and shifts in forest type and under climate change agree with other modeling studies in this region. For example, both AFRESCO-TEM and ecosys predicted similar declines in spruce forests under climate change with corresponding increases in hardwoods (Euskirchen et al., 2016; Mekonnen et al., 2019). A shift from a spruce to deciduous dominated landscape, like we projected, could act as a negative feedback to increasing fire activity in boreal forests (Pastick et al., 2017), but our projections did not suggest this would happen by mid-century. Future work applying DGS in Alaska will include simulations of larger landscapes, longer durations and more climate change scenarios as they become available from CMIP6.

4.4. Model limitations

Although wildfire is likely the most important disturbance in interior Alaska, other disturbances, such as aspen leaf miner and browsing by moose and hare, may affect forest dynamics and their effects may increase under climate change. Also, exotic tree species like chokecherry may increase forest biomass while sequential droughts may reduce biomass, neither of which were included in our simulations. Simulating the effects of climate change was limited to only one climate emissions scenario due to the lack of downscaled daily climate data necessary to simulate wildfire in the SCRPPLE extension of LANDIS-II and hydrologic dynamics in SHAW. Other important sources of uncertainty in the DGS simulations include potential parameter equifinality, uncertainty in vegetative and soil initial conditions, lack of lateral water transport, and uncertainty in the climate inputs originating from differences between GCMs, downscaling and bias correction method, and aggregation to climate regions for DGS. Quantifying and constraining these uncertainty sources remains an important area for future research for process models like LANDIS-II. The new DGS extension also has considerable potential to be applied in temperate forested regions to better understand and predict disturbance and hydrology feedbacks and their consequences for ecosystem function across multiple biomes. Given the extensive data inputs required by DGS, application may be limited in areas like the tropics where data availability is a concern.

5. Conclusions

The large extent and high C storage capacity of boreal forests makes them important to global carbon budgets, but their fragility in the face of rapid changes in climate and wildfire necessitate improved understanding of the vulnerability of this large C stock. We developed DGS, a new extension of LANDIS-II, to simulate climate, vegetation succession, hydrology, permafrost, carbon and nutrient cycling, and wildfire in a spatially-explicit framework that allows for feedbacks among processes. The DGS model captures how rising temperatures can cause permafrost thaw, which can increase active layer thickness and depth to permafrost, allowing soil water to drain deeper into the soil profile. The model also simulates changes in snow depth, snowmelt and freeze-up, and tracks soil organic matter, and water and nutrient availability at user-specified depths down to 75 m. Simulating these processes in an integrated, spatially-explicit framework like LANDIS-II will allow us to disentangle the drivers and ecosystem responses in this rapidly changing ecosystem.

Supporting information

Supplemental 1. Climate change projections
Supplemental 2. Initial maps of species composition and age
Supplemental 3. Parameterization, calibration and validation of DGS
Supplemental 4. Calibration of Scrpple
All inputs and R scripts can be found on GitHub: https://github.com/LANDIS-II-Foundation/Project-Alaska-Reburns/

CRediT authorship contribution statement

Melissa S. Lucash: Conceptualization, Methodology, Data curation, Writing – original draft. **Adrienne M. Marshall:** Conceptualization, Methodology, Software, Data curation, Writing – review & editing. **Shelby A. Weiss:** Methodology, Software, Data curation, Writing – review & editing. **John W. McNabb:** Conceptualization, Methodology, Software. **Dmitry J. Nicolsky:** Methodology, Software, Data curation, Writing – review & editing. **Gerald N. Flerchinger:** Software, Writing – review & editing. **Timothy E. Link:** Conceptualization, Methodology, Writing – review & editing. **Jason G. Vogel:** Methodology, Writing – review & editing. **Robert M. Scheller:** Software, Writing – review & editing. **Rose Z. Abramoff:** Methodology, Software, Validation, Writing – review & editing. **Vladimir E. Romanovsky:** Data curation, Writing – review & editing.

Declaration of Competing Interest

The authors declare that they have no known competing financial interests or personal relationships that could have appeared to influence the work reported in this paper.

Data availability

Model code: https://github.com/LANDIS-II-Foundation/Extension-DGS-Succession. Inputs and R code : https://github.com/LANDIS-II-Foundation/Project-Alaska-Reburns/tree/master/Lucash_etal_DGS_paper

Acknowledgments

This research was funded by National Science Foundation (Grant #1737413). The authors are very grateful to the decades of data collection at the BNZ LTER, which was utilized as calibration data for this manuscript (NSF Grant #DEB-1636476). We also wish to thank James Lamping for creating our map and diagram of DGS. Comments from anonymous reviewers greatly improved the manuscript. We respectfully acknowledge that data used in this research was gathered on the ancestral and unceded traditional territories of the People of the lower Tanana Dene and the Dena'ina.

Supplementary materials

Supplementary material associated with this article can be found, in the online version, at doi:10.1016/j.ecolmodel.2023.110367.

References

Abramoff, R.Z., Davidson, E.A., Finzi, A.C., 2017. A parsimonious modular approach to building a mechanistic belowground carbon and nitrogen model. J. Geophys. Res. Biogeosci. 122, 2418–2434. https://doi.org/10.1002/2017JG003796.
Albani, M., Medvigy, D., Hurtt, G.C., Moorcroft, P.R., 2006. The contributions of land-use change, CO_2 fertilization, and climate variability to the eastern US carbon sink. Glob. Chang. Biol. 12, 2370–2390. https://doi.org/10.1111/j.1365-2486.2006.01254.x.
Alexander, H.D., Mack, M.C., 2016. A canopy shift in interior Alaskan boreal forests: consequences for above- and belowground carbon and nitrogen pools during post-fire succession. Ecosystems 19, 98–114. https://doi.org/10.1007/s10021-015-9920-7.

American Meteorological Society, 2020. Mixing Ratio. Glossary of Meterology. https://glossary.ametsoc.org/wiki/Mixing_ratio.
Anderson, E.A., 1976. A Point Energy and Mass Balance Model of a Snow Cover. Stanford University, California.
Andresen, C.G., Lawrence, D.M., Wilson, C.J., Mcguire, A.D., Koven, C., Schaefer, K., Jafarov, E., Peng, S., Chen, X., Gouttevin, I., Burke, E., Chadburn, S., Ji, D., Chen, G., Hayes, D., Zhang, W., 2020. Soil moisture and hydrology projections of the permafrost region-a model intercomparison. Cryosphere 14, 445–459. https://doi.org/10.5194/tc-14-445-2020.
Armatas, C.A., Campbell, R.M., Watson, A.E., Borrie, W.T., Christensen, N., Venn, T.J., 2018. An integrated approach to valuation and tradeoff analysis of ecosystem services for National Forest decision-making. Ecosyst. Serv. 33, 1–18.
Ayres, M.P., Lombardero, M.J., 2000. Assessing the consequences of global change for forest disturbance from herbivores and pathogens. Sci. Total Environ. 262, 263–286. https://doi.org/10.1016/S0048-9697(00)00528-3.
Bachelet, D., Lenihan, J., Neilson, R., Drapek, R., Kittel, T., 2005. Simulating the response of natural ecosystems and their fire regimes to climatic variability in Alaska. Can. J. For. Res. 35, 2244–2257. https://doi.org/10.1139/x05-086.
Balshi, M.S., McGuire, A.D., Duffy, P., Flannigan, M., Walsh, J., Melillo, J., 2009. Assessing the response of area burned to changing climate in western boreal North America using a Multivariate Adaptive Regression Splines (MARS) approach. Glob. Change Biol. 15, 578–600. https://doi.org/10.1111/j.1365-2486.2008.01679.x.
Barber, V.A., Juday, G.P., Finney, B.P., 2000. Reduced growth of Alaskan white spruce in the twentieth century from temperature-induced drought stress. Nature 405, 668–673. https://doi.org/10.1038/35015049.
Barber, V.A., Juday, G.P., Finney, B.P., Wilmking, M., 2004. Reconstruction of summer temperatures in interior Alaska from tree-ring proxies: evidence for changing synoptic climate regimes. Clim. Change 63, 91–120. https://doi.org/10.1023/B:CLIM.0000018501.98266.55.
Barichivich, J., Briffa, K., Myneni, R., Schrier, G., Dorigo, W., Tucker, C., Osborn, T., Melvin, T., 2014. Temperature and snow-mediated moisture controls of summer photosynthetic activity in northern terrestrial ecosystems between 1982 and 2011. Remote Sens. 6, 1390–1431. https://doi.org/10.3390/rs6021390.
Beaudette, D.E., Skovlin, J., Roecker, S., Beaudette, M.D.E., 2021. Package 'soilDB': soil Database Interface. R package version 2.6.12.
Berner, L.T., Alexander, H.D., Loranty, M.M., Ganzlin, P., Mack, M.C., Davydov, S.P., Goetz, S.J., 2015. Biomass allometry for alder, dwarf birch, and willow in boreal forest and tundra ecosystems of far northeastern Siberia and north-central Alaska. For. Ecol. Manag. 337, 110–118. https://doi.org/10.1016/j.foreco.2014.10.027.
Bernhardt, E.L., Hollingsworth, T.N., Chapin, F., Stuart, I.I.I., 2011. Fire severity mediates climate-driven shifts in understorey community composition of black spruce stands of interior Alaska. J. Veg. Sci. 22, 32–44. https://doi.org/10.1111/j.1654-1103.2010.01231.x.
Bieniek, P.A., Bhatt, U.S., Walsh, J.E., Rupp, T.S., Zhang, J., Krieger, J.R., Lader, R., 2016. Dynamical downscaling of ERA-interim temperature and precipitation for. Alaska. J. Appl. Meteorol. Climatol. 55, 635–654. https://doi.org/10.1175/JAMC-D-15-0153.1.
Bieniek, P.A., Walsh, J.E., Thoman, R.L., Bhatt, U.S., 2014. Using climate divisions to analyze variations and trends in Alaska temperature and precipitation. J. Clim. 27, 2800–2818. https://doi.org/10.1175/JCLI-D-13-00342.1.
Black, R.F., 1951. Eolian deposits of Alaska. Arctic 4, 89–111.
Bonan, G.B., 1991. A biophysical surface energy budget analysis of soil temperature in the boreal forests of interior Alaska. Water Resour. Res. 27, 767–781.
Bonan, G.B., Shugart, H.H., 1989. Environmental factors and ecological processes in boreal forests. Annu. Rev. Ecol. Syst. 20, 1–28.
Bradshaw, C.J.A., Warkentin, I.G., 2015. Global estimates of boreal forest carbon stocks and flux. Glob. Planet. Change 128, 24–30. https://doi.org/10.1016/j.gloplacha.2015.02.004.
Brown, C.D., Johnstone, J.F., 2012. Once burned, twice shy: repeat fires reduce seed availability and alter substrate constraints on *Picea mariana* regeneration. For. Ecol. Manag. 266, 34–41. https://doi.org/10.1016/j.foreco.2011.11.006.
Buma, B., Brown, C.D., Donato, D.C., Fontaine, J.B., Johnstone, J.F., 2013. The impacts of changing disturbance regimes on serotinous plant populations and communities. Bioscience 63, 866–876. https://doi.org/10.1525/bio.2013.63.11.5.
Buma, B., Hayes, K., Weiss, S., Lucash, &.M., 2022. Short-interval fires increasing in the Alaskan boreal forest as fire self-regulation decays across forest types. Sci. Rep. 12, 4901. https://doi.org/10.1038/s41598-022-08912-8.
Burns, R.M., Honkala, B.H., 1990. Silvics of North America. Volume 2: Hardwoods. Agriculture Handbook 654. USDA Forest Service.
Burrill, E.A., Wilson, A.M., Turner, J.A., Pugh, S.A., Menlove, J., Christensen, G., Conkling, B.L., David, W., 2018. FIA database description and user guide for phase 2 (version: 8.0).
Burt, R., 2009. Soil Survey Field and Laboratory Methods Manual (Soil Survey Investigations Report No. 51, Version 1.0). USDA-NRCS. National Soil Survey Center, Lincoln, NE.
Cable, J.M., Ogle, K., Bolton, W.R., Bentley, L.P., Romanovsky, V., Iwata, H., Harazono, Y., Welker, J., 2014. Permafrost thaw affects boreal deciduous plant transpiration through increased soil water, deeper thaw, and warmer soils. Ecohydrology 7, 982–997. https://doi.org/10.1002/eco.1423.
Calef, M.P., Varvak, A., McGuire, A.D., Chapin, F.S., Reinhold, K.B., 2015. Recent changes in annual area burned in interior Alaska: the impact of fire management. Earth Interact. 19, 1–17. https://doi.org/10.1175/EI-D-14-0025.1.
Chauvin, G.M., Flerchinger, G.N., Link, T.E., Marks, D., Winstral, A.H., Seyfried, M.S., 2011. Long-term water balance and conceptual model of a semi-arid mountainous catchment. J. Hydrol. 400, 133–143.
Clow, G.D., 2008. Continued permafrost warming in northwest Alaska as detected by the DOI/GTN-P borehole array. In: Kane, D.L., Hinkel, K.M. (Eds.), Ninth International Conference on Permafrost, Extended Abstracts. Institute of Northern Engineering, University of Alaska, Fairbanks, AK, pp. 47–48.
Coogan, S.C.P., Cai, X., Jain, P., Flannigan, M.D., 2020. Seasonality and trends in human- and lightning-caused wildfires ≥ 2 ha in Canada, 1959–2018. Int. J. Wildl. Fire 29, 473–485.
Dai, A., Trenberth, K.E., Qian, T., 2004. A global dataset of Palmer Drought Severity Index for 1870–2002: relationship with soil moisture and effects of surface warming. J. Hydrometeorol. 5, 1117–1130. https://doi.org/10.1175/JHM-386.1.
Davidson, E.A., Samanta, S., Caramori, S.S., Savage, K., 2012. The dual Arrhenius and Michaelis–Menten kinetics model for decomposition of soil organic matter at hourly to seasonal time scales. Glob. Chang. Biol. 18, 371–384. https://doi.org/10.1111/j.1365-2486.2011.02546.x.
Davidson, E.A., Savage, K.E., Finzi, A.C., 2014. A big-microsite framework for soil carbon modeling. Glob. Chang. Biol. 20, 3610–3620. https://doi.org/10.1111/GCB.12718.
Debolskiy, M.V., Nicolsky, D.J., Hock, R., Romanovsky, V.E., 2020. Modeling present and future permafrost distribution at the Seward Peninsula. Alaska. J. Geophys. Res. Earth Surf. 125 (8), e2019JF005355 https://doi.org/10.1029/2019JF005355.
Dimitrov, D.D., Grant, R.F., Lafleur, P.M., Humphreys, E.R., 2010. Modeling the effects of hydrology on ecosystem respiration at Mer Bleue bog. J. Geophys. Res. Biogeosci. 115 https://doi.org/10.1029/2010JG001312.
Duffy, P., Walsh, J.E., Mann, D.H., Graham, J.M., Rupp, T.S., 2005. Impacts of large-scale atmospheric–ocean variability on Alaskan fire season severity. Ecol. Appl. 15, 1317–1330.
Dymond, C.C., Beukema, S., Nitschke, C.R., David Coates, K., Scheller, R.M., 2016. Carbon sequestration in managed temperate coniferous forests under climate change. Biogeosciences 13, 1933–1947. https://doi.org/10.5194/bg-13-1933-2016.
Dyrness, C.T., 1982. Control of depth to permafrost and soil temperature by the forest floor in black spruce/feathermoss communities. USDA For. Serv. Pac. Northwest For. and Range Exp. Stn., Res. Note, pp. 1–19. PNW-396.
Edwards, M.E., Brubaker, L.B., Lozhkin, A.V., Anderson, P.M., 2005. Structurally novel biomes: a response to past warming in Beringia. Ecology 86, 1696–1703.
Eliasson, P.E., McMurtrie, R.E., Pepper, D.A., Stromgren, M., Linder, S., Agren, G.I., 2005. The response of heterotrophic CO_2 flux to soil warming. Glob. Chang. Biol. 11, 167–181. https://doi.org/10.1111/j.1365-2486.2004.00878.x.
Euskirchen, E.S., Bennett, A.P., Breen, A.L., Genet, H., Lindgren, M.A., Kurkowski, T.A., McGuire, A.D., Rupp, T.S., 2016. Consequences of changes in vegetation and snow cover for climate feedbacks in Alaska and northwest Canada. Environ. Res. Lett. 11, 105003 https://doi.org/10.1088/1748-9326/11/10/105003.
Euskirchen, E.S., Bret-Harte, M.S., Shaver, G.R., Edgar, C.W., Romanovsky, V.E., 2017. Long-term release of carbon dioxide from arctic tundra ecosystems in Alaska. Ecosystems 20, 960–974. https://doi.org/10.1007/s10021-016-0085-9.
Euskirchen, E.S., Mcguire, A.D., Chapin, F.S., Yi, S., Thompson, C.C., 2009. Changes in vegetation in northern Alaska under scenarios of climate change, 2003-2100: implications for climate feedbacks. Ecol. Appl. 19, 1022–1043.
Euskirchen, E.S., McGuire, A.D., Chapin III, F.S., 2007. Energy feedbacks of northern high-latitude ecosystems to the climate system due to reduced snow cover during 20th century warming. Glob. Chang. Biol. 13, 2425–2438.
Euskirchen, E.S., McGuire, A.D., Kicklighter, D.W., Zhuang, Q., Clein, J.S., Dargaville, R. J., Dye, D.G., Kimball, J.S., McDonald, K.C., Melillo, J.M., Romanovsky, V.E., Smith, N.V., 2006. Importance of recent shifts in soil thermal dynamics on growing season length, productivity, and carbon sequestration in terrestrial high-latitude ecosystems. Glob. Chang. Biol. 12, 731–750. https://doi.org/10.1111/j.1365-2486.2006.01113.x.
Farouki, O.T., 1981. The thermal properties of soils in cold regions. Cold Reg. Sci. Technol. 5, 67–75. https://doi.org/10.1016/0165-232X(81)90041-0.
Finzi, A.C., Abramoff, R.Z., Spiller, K.S., Brzostek, E.R., Darby, B.A., Kramer, M.A., Phillips, R.P., 2015. Rhizosphere processes are quantitatively important components of terrestrial carbon and nutrient cycles. Glob. Chang. Biol. 21, 2082–2094. https://doi.org/10.1111/GCB.12816.
Flannigan, M., Stocks, B., Turetsky, M., Wotton, M., 2009a. Impacts of climate change on fire activity and fire management in the circumboreal forest. Glob. Chang. Biol. 15, 549–560. https://doi.org/10.1111/j.1365-2486.2008.01660.x.
Flannigan, M.D., Krawchuk, M.A., de Groot, W.J., Wotton, B.M., Gowman, L.M., 2009b. Implications of changing climate for global wildland fire. Int. J. Wildl. fire 18, 483–507.
Flerchinger, G.N., Cooley, K.R., 2000. A ten-year water balance of a mountainous semi-arid watershed. J. Hydrol. 237, 86–99. https://doi.org/10.1016/S0022-1694(00)00299-7.
Flerchinger, G.N., Cooley, K.R., Deng, Y., 1994. Impacts of spatially and temporally varying snowmelt on subsurface flow in a mountainous watershed: 1. Snowmelt simulation. Hydrol. Sci. J. 39, 507–520. https://doi.org/10.1080/02626669409492771.
Flerchinger, G.N., Reba, M.L., Link, T.E., Marks, D., 2016. Modeling temperature and humidity profiles within forest canopies. Agric. For. Meteorol. 213, 251–262. https://doi.org/10.1016/j.agrformet.2015.07.007.
Flerchinger, G.N., Saxton, K.E., 1989. Simultaneous heat and water model of a freezing snow-residue-soil system II. Field verification. Trans. ASAE 32, 573–576.
Foster, A.C., Armstrong, A.H., Shuman, J.K., Shugart, H.H., Rogers, B.M., Mack, M.C., Goetz, S.J., Ranson, K.J., 2019. Importance of tree- and species-level interactions with wildfire, climate, and soils in interior Alaska: implications for forest change under a warming climate. Ecol. Modell. 409, 108765 https://doi.org/10.1016/j.ecolmodel.2019.108765.
Foster, A.C., Shuman, J.K., Rogers, B.M., Walker, X.J., Mack, M.C., Bourgeau-Chavez, L. L., Veraverbeke, S., Goetz, S.J., 2022. Bottom-up drivers of future fire regimes in

western boreal North America. Environ. Res. Lett. 17, 025006 https://doi.org/10.1088/1748-9326/ac4c1e.
Genet, H., McGuire, A.D., Barrett, K., Breen, A., Euskirchen, E.S., Johnstone, J.F., Kasischke, E.S., Melvin, A.M., Bennett, A., Mack, M.C., Rupp, T.S., Schuur, G., Turetsky, A.E., Yuan, F, M.R., 2013. Modeling the effects of fire severity and climate warming on active layer thickness and soil carbon storage of black spruce forests across the landscape in interior Alaska. Environ. Res. Lett. 8, 45016–45029. https://doi.org/10.1088/1748-9326/8/4/045016.
GeoMAC, 2020. Historic Perimeters 2019. U.S. Geological Survey. https://data-nifc.opendata.arcgis.com/datasets/nifc::historic-perimeters-2019/about. accessed 8.15.20.
GeoMAC, 2019. Historic Perimeters Combined 2000-2018. U.S. Geological Survey. https://data-nifc.opendata.arcgis.com/datasets/nifc::historic-perimeters-combined-2000-2018/about. accessed 8.15.20.
Goetz, S.J., Bunn, A.G., Fiske, G.J., Houghton, R.A., 2005. Satellite-observed photosynthetic trends across boreal North America associated with climate and fire disturbance. Proc. Natl. Acad. Sci. 102, 13521–13525.
Gower, S.T., Krankina, O., Olson, R.J., Apps, M., Linder, S., Wang, C., 2001. Net primary production and carbon allocation patterns of boreal forest ecosystems. Ecol. Appl. 11, 1395. https://doi.org/10.2307/3060928.
Gudmundsson, L., Gudmundsson, M.L., 2012. Package 'qmap.' methods 2012, 3383–3390.
Gustafson, E.J., Shvidenko, A.Z., Scheller, R.M., 2011. Effectiveness of forest management strategies to mitigate effects of global change in south-central Siberia. Can. J. For. Res. 41, 1405–1421. https://doi.org/10.1139/X11-065.
Gustafson, E.J., Shvidenko, A.Z., Sturtevant, B.R., Scheller, R.M., 2010. Predicting global change effects on forest biomass and composition in south-central Siberia. Ecol. Appl. 20, 700–715. https://doi.org/10.1890/08-1693.1/FORMAT/PDF.
Hansen, W.D., Fitzsimmons, R., Olnes, J., Williams, A.P., 2021. An alternate vegetation type proves resilient and persists for decades following forest conversion in the North American boreal biome. J. Ecol. 109, 85–98. https://doi.org/10.1111/1365-2745.13446.
He, H., Flerchinger, G.N., Kojima, Y., He, D., Hardegree, S.P., Dyck, M.F., Horton, R., Wu, Q., Si, B., Lv, J., Wang, J., 2021. Evaluation of 14 frozen soil thermal conductivity models with observations and SHAW model simulations. Geoderma 403. https://doi.org/10.1016/J.GEODERMA.2021.115207.
Hesketh, M., Greene, D.F., Pounden, E., 2009. Early establishment of conifer recruits in the northern Rocky Mountains as a function of postfire duff depth. Can. J. For. Res. 39, 2059–2064. https://doi.org/10.1139/X09-120.
Higuera, P.E., Brubaker, L.B., Anderson, P.M., Sheng, F.H., Brown, T.A., 2009. Vegetation mediated the impacts of postglacial climate change on fire regimes in the south-central Brooks Range. Ecol. Monogr. 79, 201–219.
Hinzman, L.D., Bettez, N.D., Bolton, W.R., Chapin, F.S., Dyurgerov, M.B., Fastie, C.L., Griffith, B., Hollister, R.D., Hope, A., Huntington, H.P., Jensen, A.M., Jia, G.J., Jorgenson, T., Kane, D.L., Klein, D.R., Kofinas, G., Lynch, A.H., Lloyd, A.H., McGuire, A.D., Nelson, F.E., Oechel, W.C., Osterkamp, T.E., Racine, C.H., Romanovsky, V.E., Stone, R.S., Stow, D.A., Sturm, M., Tweedie, C.E., Vourlitis, G.L., Walker, M.D., Walker, D.A., Webber, P.J., Welker, J.M., Winker, K.S., Yoshikawa, K., 2005. Evidence and implications of recent climate change in northern Alaska and other Arctic regions. Clim. Change 72, 251–298. https://doi.org/10.1007/s10584-005-5352-2.
Hinzman, L.D., Chapin, F.S., Fukuda, M., 2013. Current fire regimes, impacts and the likely changes – III : boreal permafrost biomes. Veg. Fires Glob. Chang. Challenges Concert. Int. Action 79–88.
Hinzman, L.D., Viereck, L.A., Adams, P.C., Romanovsky, V.E., Yoshikawa, K., 2006. Climate and permafrost dynamics of the Alaskan boreal forest. Eds.. In: Chapin, F.S., Oswood, M.W., van Cleve, K., Viereck, L.A., Verbyla, D.L. (Eds.), Alaska's Changing Boreal Forest. Oxford University Press, pp. 39–61.
Hobbie, S.E., Nadelhoffer, K.J., Högberg, P., 2002. A synthesis: the role of nutrients as constraints on carbon balances in boreal and arctic regions. Plant Soil 242, 163–170. https://doi.org/10.1023/A:1019670731128.
Hobbie, S.E., Schimel, J.P., Trumbore, S.E., Randerson, J.R., 2000. Controls over carbon storage and turnover in high-latitude soils. Glob. Chang. Biol. 6, 196–210. https://doi.org/10.1046/j.1365-2486.2000.06021.x.
Hoecker, T.J., Higuera, P.E., Kelly, R., Hu, F.S., 2020. Arctic and boreal paleofire records reveal drivers of fire activity and departures from Holocene variability. Ecology 101. https://doi.org/10.1002/ecy.
Hoy, E.E., Turetsky, M.R., Kasischke, E.S., 2016. More frequent burning increases vulnerability of Alaskan boreal black spruce forests. Environ. Res. Lett. 11 https://doi.org/10.1088/1748-9326/11/9/095001.
Isaksen, K., Ødegård, R.S., Etzelmüller, B., Hilbich, C., Hauck, C., Farbrot, H., Eiken, T., Hygen, H.O., Hipp, T.F., 2011. Degrading mountain permafrost in southern Norway: spatial and temporal variability of mean ground temperatures, 1999-2009. Permafr. Periglac. Process. 22, 361–377. https://doi.org/10.1002/ppp.728.
Jackman et al., 2015S. Jackman, A. Tahk, A. Zeileis, C. Maimone, J. Fearon, Z. Meers, M. Simon, M.A.S.S. ImportsPackage .. pscl...Political Science Computational Laboratory (2015)18(04.2017).
Jafarov, E.E., Marchenko, S.S., Romanovsky, V.E., 2012. Numerical modeling of permafrost dynamics in Alaska using a high spatial resolution dataset. Cryosphere 6, 613–624. https://doi.org/10.5194/tc-6-613-2012.
Jafarov, E.E., Romanovsky, V.E., Genet, H., McGuire, A.D., Marchenko, S.S., 2013. The effects of fire on the thermal stability of permafrost in lowland and upland black spruce forests of interior Alaska in a changing climate. Environ. Res. Lett. 8, 035030 https://doi.org/10.1088/1748-9326/8/3/035030.
Jarvis, P.J., 1976. The interpretation of the variations in leaf water potential and stomatal conductance found in canopies in the field. Trans. R. Soc. Lond. B 273, 593–610.
Jasechko, S., Sharp, Z.D., Gibson, J.J., Birks, S.J., Yi, Y., Fawcett, P.J., 2013. Terrestrial water fluxes dominated by transpiration. Nature 496, 347–350. https://doi.org/10.1038/NATURE11983.
Jasinski, J.P.P., Payette, S., 2005. The creation of alternative stable states in the southern boreal forest, Quebec, Canada. Ecol. Monogr. 75, 561–583. https://doi.org/10.1890/04-1621.
Johnstone, J.F., Chapin, F.S., 2006. Fire interval effects on successional trajectory in boreal forests of northwest Canada. Ecosystems 9, 268–277. https://doi.org/10.1007/s10021-005-0061-2.
Johnstone, J.F., Chapin, F.S., Hollingsworth, T.N., Mack, M.C., Romanovsky, V., Turetsky, M., 2010a. Fire, climate change, and forest resilience in interior Alaska. Can. J. For. Res. 40, 1302–1312. https://doi.org/10.1139/X10-061.
Johnstone, J.F., Hollingsworth, T.N., Chapin, F.S., Mack, M.C., 2010b. Changes in fire regime break the legacy lock on successional trajectories in Alaskan boreal forest. Glob. Chang. Biol. 16, 1281–1295. https://doi.org/10.1111/j.1365-2486.2009.02051.x.
Jolly, W.M., Cochrane, M.A., Freeborn, P.H., Holden, Z.A., Brown, T.J., Williamson, G.J., Bowman, D.M.J.S., 2015. Climate-induced variations in global wildfire danger from 1979 to 2013. Nat. Commun. https://doi.org/10.1038/ncomms8537.
Jorgenson, M.T., Racine, C.H., Walters, J.C., Osterkamp, T.E., 2001. Permafrost degradation and ecological changes associated with a warming climate in central Alaska. Clim. Change 48, 551–579. https://doi.org/10.1023/A:1005667424292.
Jorgenson, M.T., Romanovsky, V., Harden, J., Shur, Y., Donnell, J.O., Schuur, E.A.G., Kanevskiy, M., 2010. Resilience and vulnerability of permafrost to climate change. Can. J. For. Res. 40, 1219–1236. https://doi.org/10.1139/X10-060.
Ju, J., Masek, J.G., 2016. The vegetation greenness trend in Canada and US Alaska from 1984 to 2012 Landsat data. Remote Sens. Environ. 176, 1–16. https://doi.org/10.1016/j.rse.2016.01.001.
Kasischke, E.S., Turetsky, M.R., 2006. Recent changes in the fire regime across the North American boreal region - Spatial and temporal patterns of burning across Canada and Alaska. Geophys. Res. Lett. 33 https://doi.org/10.1029/2006GL025677.
Kasischke, E.S., Verbyla, D.L., Rupp, T.S., Mcguire, A.D., Murphy, K.A., Jandt, R., Barnes, J.L., Hoy, E.E., Duffy, P.A., Calef, M., Turetsky, M.R., 2010. Alaska's changing fire regime - implications for the vulnerability of its boreal forests. Can. J. For. Res. 40, 1313–1324.
Keeley, J.E., Ne'eman, G., Fotheringham, C.J., 1999. Immaturity risk in a fire-dependent pine. J. Mediterr. Ecol. 1, 41–48.
Keenan, T.F., Luo, X., De Kauwe, M.G., Medlyn, B.E., Prentice, I.C., Stocker, B.D., Smith, N.G., Terrer, C., Wang, H., Zhang, Y., Zhou, S., 2021. A constraint on historic growth in global photosynthesis due to increasing CO_2. Nature 600, 253–258. https://doi.org/10.1038/s41586-021-04096-9.
Kelly, R., Chipman, M.L., Higuera, P.E., Stefanova, I., Brubaker, L.B., Hu, F.S., 2013. Recent burning of boreal forests exceeds fire regime limits of the past 10,000 years. PNAS 110, 13055–13060. https://doi.org/10.1073/pnas.1305069110.
Koven, C.D., Riley, W.J., Stern, A., 2013. Analysis of permafrost thermal dynamics and response to climate change in the CMIP5 Earth System Models. J. Clim. 26, 1877–1900. https://doi.org/10.1175/JCLI-D-12-00228.1.
Koven, C.D., Ringeval, B., Friedlingstein, P., Ciais, P., Cadule, P., Khvorostyanov, D., Krinner, G., Tarnocai, C., 2011. Permafrost carbon-climate feedbacks accelerate global warming. Proc. Natl. Acad. Sci. U.S.A. 108, 14769–14774. https://doi.org/10.1073/pnas.1103910108.
L'Heureux, M., Mann, M.E., Cook, B.I., Gleason, B.E., Vose, R.S., 2004. Atmospheric circulation influences on seasonal precipitation patterns in Alaska during the latter 20th century. J. Geophys. Res. 109, 6106. https://doi.org/10.1029/2003JD003845.
Lader, R., Walsh, J.E., Bhatt, U.S., Bieniek, P.A., 2020. Anticipated changes to the snow season in Alaska: elevation dependency, timing and extremes. Int. J. Climatol. 40, 169–187. https://doi.org/10.1002/joc.6201.
Lader, R., Walsh, J.E., Bhatt, U.S., Bieniek, P.A., 2017. Projections of twenty-first-century climate extremes for Alaska via dynamical downscaling and quantile mapping. J. Appl. Meteorol. Climatol. 56, 2393–2409. https://doi.org/10.1175/JAMC-D-16-0415.1.
Leonawicz, M., Lindgren, M., Kurkowski, T., Walsh, J., Rupp, S., 2015. Projected monthly and derived temperature products - 771M CMIP5/AR5. Fairbanks, AK.
Link, T.E., Flerchinger, G.N., Unsworth, M., Marks, D., 2004. Simulation of water and energy fluxes in an old-growth seasonal temperate rain forest using the Simultaneous Heat and Water (SHAW) model. J. Hydrometeorol. 5, 443–457. https://doi.org/10.1175/1525-7541(2004)005<0443:SOWAEF>2.0.CO;2.
Liu, H., Randerson, J.T., Lindfors, J., Stuart, F., Iii, C., 2005. Changes in the surface energy budget after fire in boreal ecosystems of interior Alaska: an annual perspective. J. Geophys. Res. 110, 13101. https://doi.org/10.1029/2004JD005158.
Lucash, M.S., Scheller, R.M., 2021. LANDIS-II Climate Library v4.2 User Guide.
Lynch, J.A., Clark, J.S., Bigelow, N.H., Edwards, M.E., Finney, B.P., 2003. Geographic and temporal variations in fire history in boreal ecosystems of Alaska. J. Geophys. Res. Atmos. 108 https://doi.org/10.1029/2001JD000332/FORMAT/PDF.
Malkova, G.V., 2010. Mean-annual ground temperature monitoring on the steady-state station "Bolvansky". Earth Cryosph. 14, 3–14.
Mann, D., Rupp, T., Olson, M., Duffy, P., 2012. Is Alaska's boreal forest now crossing a major ecological threshold? Arctic, Antarct. Alp. Res. 44, 319–331. https://doi.org/10.1657/1938-4246-44.3.319.
Marchenko, S., Romanovsky, V., Tipenko, G., 2008. Numerical modeling of spatial permafrost dynamics in Alaska. In: Proceedings of the Ninth International Conference on Permafrost. Institute of Northern Engineering, University of Alaska Fairbanks, pp. 1125–1130.
Markon, C., Gray, S., Berman, M., Eerkes-Medrano, L., Hennessy, T., Huntington, H., Littell, J., McCammon, M., Thoman, R., Trainor, S., 2018. Alaska: Impacts, risks, and

adaptation in the United States. Fourth National Climate Assessment, Washington, DC, USA. https://doi.org/10.7930/NCA4.2018.CH26.
Marquis, D.A., Solomon, D.S., Bjorkbom, J.C., 1969. A silvicultural guide for paper birch in the northeast. US Department of Agriculture, Forest Service, Northeastern Forest Experiment Station Research Paper NE-130.
Marshall, A.M., Link, T.E., Abatzoglou, J.T., Flerchinger, G.N., Marks, D.G., Tedrow, L., 2019. Warming alters hydrologic heterogeneity: simulated climate sensitivity of hydrology-based microrefugia in the snow-to-rain transition zone. Water Resour. Res. 55, 2122–2141. https://doi.org/10.1029/2018WR023063.
Marshall, A.M., Link, T.E., Flerchinger, G.N., Lucash, M.S., 2021a. Importance of parameter and climate data uncertainty for future changes in boreal hydrology. Water Resour. Res. 57, 1–20. https://doi.org/10.1029/2021WR029911.
Marshall, A.M., Link, T.E., Flerchinger, G.N., Nicolsky, D.J., Lucash, M.S., 2021b. Ecohydrological modelling in a deciduous boreal forest: model evaluation for application in non-stationary climates. Hydrol. Process. 35, e14251. https://doi.org/10.1002/HYP.14251.
McAfee, S.A., Guentchev, G., Eischeid, J.K., 2013. Reconciling precipitation trends in Alaska: 1. Station-based analyses. J. Geophys. Res. Atmos. 118, 7523–7541. https://doi.org/10.1002/jgrd.50572.
McCaughey, W.W., Schmidt, W.C., Shearer, R.C., 1986. In: Shearer, R.C. (Ed.), Conifer tree seed in the Inland Mountain West symposium. General Technical Report, INT-GTR-203. USDA Forest Service, Intermountain Research Station, Missoula, MT, pp. 50–62.
McGuire, A.D., Lawrence, D.M., Koven, C., Clein, J.S., Burke, E., Chen, G., Jafarov, E., MacDougall, A.H., Marchenko, S., Nicolsky, D., Peng, S., Rinke, A., Ciais, P., Gouttevin, I., Hayes, D.J., Ji, D., Krinner, G., Moore, J.C., Romanovsky, V., Schädel, C., Schaefer, K., Schuur, E.A.G., Zhuang, Q., 2018. Dependence of the evolution of carbon dynamics in the northern permafrost region on the trajectory of climate change. Proc. Natl. Acad. Sci. U.S.A. 115, 3882–3887. https://doi.org/10.1073/pnas.1719903115.
Mekonnen, Z.A., Riley, W.J., Randerson, J.T., Grant, R.F., Rogers, B.M., 2019. Expansion of high-latitude deciduous forests driven by interactions between climate warming and fire. Nat. Plants 5, 952–958. https://doi.org/10.1038/s41477-019-0495-8.
Melillo, J.M., Frey, S.D., DeAngelis, K.M., Werner, W.J., Bernard, M.J., Bowles, F.P., Pold, G., Knorr, M.A., Grandy, A.S., 2017. Long-term pattern and magnitude of soil carbon feedback to the climate system in a warming world. Science 358, 101–105. https://doi.org/10.1126/SCIENCE.AAN2874, 80-.
Menne, M.J., Durre, I., Vose, R.S., Gleason, B.E., Houston, T.G., 2012. An overview of the global historical climatology network-daily database. J. Atmos. Ocean. Technol. 29, 897–910. https://doi.org/10.1175/JTECH-D-11-00103.1.
Meredith, E.P., Ulbrich, U., Rust, H.W., 2019. The diurnal nature of future extreme precipitation intensification. Geophys. Res. Lett. 46, 7680–7689. https://doi.org/10.1029/2019GL082385.
Maechler, M., Rousseeuw, P., Struyf, A., Hubert, M., Hornik, K. 2022. cluster: Cluster Analysis Basics and Extensions. R package version 2.1.4.
Minsley, B.J., Pastick, N.J., Wylie, B.K., Brown, D.R.N., Andy Kass, M., 2016. Evidence for nonuniform permafrost degradation after fire in boreal landscapes. J. Geophys. Res. Earth Surf. 121, 320–335. https://doi.org/10.1002/2015JF003781/FORMAT/PDF.
Mladenoff, D.J., 2004. LANDIS and forest landscape models. Ecol. Modell. 180, 7–19. https://doi.org/10.1016/j.ecolmodel.2004.03.016.
Natalia, S., Lieffers, V.J., Landhäusser, S.M., 2008. Effects of leaf litter on the growth of boreal feather mosses: implication for forest floor development. J. Veg. Sci. 19, 253–260. https://doi.org/10.3170/2008-8-18367.
Nicolsky, D.J., Romanovsky, V.E., Alexeev, V.A., Lawrence, D.M., 2007. Improved modeling of permafrost dynamics in a GCM land-surface scheme. Geophys. Res. Lett. 34, 2–6. https://doi.org/10.1029/2007GL029525.
Nicolsky, D.J., Romanovsky, V.E., Panda, S.K., Marchenko, S.S., Muskett, R.R., 2017. Applicability of the ecosystem type approach to model permafrost dynamics across the Alaska North Slope. J. Geophys. Res. Earth Surf. 122, 50–75. https://doi.org/10.1002/2016JF003852.
Nicolsky, D.J., Romanovsky, V.E., Panteleev, G.G., Geopl, A., 2009. Estimation of soil thermal properties using in-situ temperature measurements in the active layer and permafrost. Cold Reg. Sci. Technol. 55, 120–129. https://doi.org/10.1016/j.coldregions.2008.03.003.
Noguchi, K., Dannoura, M., Jomura, M., Awazuhara-Noguchi, M., Matsuura, Y., 2012. High belowground biomass allocation in an upland black spruce (*Picea mariana*) stand in interior Alaska. Polar Sci. 6, 133–141. https://doi.org/10.1016/j.polar.2011.12.002.
Oberman, N.G., 2008. Contemporary permafrost degradation of the european north of Russia. In: Kane, D, Hinkel, K (Eds.), Ninth International Conference on Permafrost. Institute of Northern Engineering, University of Alaska Fairbanks, Fairbanks, Alaska, pp. 1305–1310. EdPp.
Osterkamp, T.E., Romanovsky, V.E., 1999. Evidence for warming and thawing of discontinuous permafrost in Alaska. Permafr. Periglac. Process. 10, 1737. https://doi.org/10.1002/(SICI)1099-1530(199901/03)10:1<17:. AID-PPP303>3.0.CO;2-4.
Overland, J.E., Hanna, E., Hanssen-Bauer, I., Kim, S.-J., Walsh, J.E., Wang, M., Bhatt, U. S., Thoman, R.L., 2018. Surface air temperature. Arctic report card 10-16.
Overpeck, J., Hughen, K., Hardy, D., Bradley, R., Case, R., Douglas, M., Finney, B., Gajewski, K., Jacoby, G., Jennings, A., Lamoureux, S., Lasca, A., Macdonald, G., Moore, J., Retelle, M., Smith, S., Wolfe, A., Zielinski, G., 1997. Arctic environmental change of the last four centuries. Science 278, 1251–1256.
Parton, W.J., Ojima, D.S., Cole, C.V., Schimel, D.S., 1994. A general model for soil organic matter dynamics: sensitivity to litter chemistry, texture and management. Quant. Model. Soil Form. Process. 39, 147–167.
Parton, W.J., Stewart, J.W.B., Cole, C.V., 1988. Dynamics of C, N, P and S in grassland soils: a model. Biogeochemistry 5, 109–131. https://doi.org/10.1007/BF02180320.
Pastick, N.J., Duffy, P., Genet, H., Rupp, T.S., Wylie, B.K., Johnson, K.D., Jorgenson, M. T., Bliss, N., McGuire, A.D., Jafarov, E.E., Knight, J.F., 2017. Historical and projected trends in landscape drivers affecting carbon dynamics in Alaska. Ecol. Appl. 27, 1383–1402. https://doi.org/10.1002/eap.1538.
Payette, S., 1992. Fire as a Controlling Process in the North American Boreal Forest. A Systems Analysis of the Global Boreal Forest. Cambridge University Press, pp. 144–169. https://doi.org/10.1017/CBO9780511565489.006.
Pewe, T.L., Bell, J.W., Forbes, R.B., Weber, F.R., 1976. Geologic Map of the Fairbanks D-2 SE Quadrangle, Alaska.
Piao, S., Sitch, S., Ciais, P., Friedlingstein, P., Peylin, P., Wang, X., Ahlström, A., Anav, A., Canadell, J.G., Cong, N., Huntingford, C., Jung, M., Levis, S., Levy, P.E., Li, J., Lin, X., Lomas, M.R., Lu, M., Luo, Y., Ma, Y., Myneni, R.B., Poulter, B., Sun, Z., Wang, T., Viovy, N., Zaehle, S., Zeng, N., 2013. Evaluation of terrestrial carbon cycle models for their response to climate variability and to CO_2 trends. Glob. Chang. Biol. 19, 2117–2132. https://doi.org/10.1111/gcb.12187.
PRISM Climate Group: Oregon State University, 2021. Recent 30 Year Normals (1981-2021). Oregon State University.
R Core Team, 2022. R: A language and environment for statistical computing. R Foundation for Statistical Computing, Vienna, Austria. https://www.R-project.org/.
Rebain, S., 2010. The fire and fuels extension to the forest vegetation simulator: updated model documentation. USDA For. Serv. For. Manag. Serv. Center, Intern. Rep., p. 396
Richardson, L.F., 1922. Weather Prediction By Numerical Process, 2nd ed. Cambridge University Press. https://doi.org/10.1017/CBO9780511618291.
Rogers, B.M., Soja, A.J., Goulden, M.L., Randerson, J.T., 2015. Influence of tree species on continental differences in boreal fires and climate feedbacks. Nat. Geosci. 8, 228–234. https://doi.org/10.1038/ngeo2352.
Romanovsky, V.E., Osterkamp, T.E., 2000. Effects of unfrozen water on heat and mass transport processes in the active layer and permafrost. Permafr. Periglac. Process 219–239. https://doi.org/10.1002/1099-1530(200007/09)11, 3<219:: AID−PPP352>3.0.CO;2-7.
Romanovsky, V.E., Smith, S.L., Isaksen, K., Shiklomanov, N.I., Streletskiy, D.A., Kholodov, A.L., Christiansen, H.H., Drozdov, D.S., Malkova, G.V., Marchenko, S.S., 2019. Terrestrial Permafrost [in "State of the Climate in 2018"]. Bulletin of the American Meteorological Society.
Rupp, T.S., Chen, X., Olson, M., McGuire, A.D., 2007. Sensitivity of simulated boreal fire dynamics to uncertainties in climate drivers. Earth Interact. 11, 1–21.
Santoro, M., 2018. GlobBiomass - global datasets of forest biomass. 10.1594/PANGAEA.894711.
Scheller, R., Kretchun, A., Hawbaker, T.J., Henne, P.D., 2019. A landscape model of variable social-ecological fire regimes. Ecol. Modell. 401, 85–93. https://doi.org/10.1016/J.ECOLMODEL.2019.03.022.
Scheller, R.M., Domingo, J.B., Sturtevant, B.R., Williams, J.S., Rudy, A., Gustafson, E.J., Mladenoff, D.J., 2007. Design, development, and application of LANDIS-II, a spatial landscape simulation model with flexible temporal and spatial resolution. Ecol. Modell. 201, 409–419. https://doi.org/10.1016/j.ecolmodel.2006.10.009.
Scheller, R.M., Hua, D., Bolstad, P.V., Birdsey, R.A., Mladenoff, D.J., 2011. The effects of forest harvest intensity in combination with wind disturbance on carbon dynamics in Lake States Mesic Forests. Ecol. Modell. 222, 144–153. https://doi.org/10.1016/j.ecolmodel.2010.09.009.
Scheller, R.M., Kretchun, A.M., Van Tuyl, S., Clark, K.L., Lucash, M.S., Hom, J., 2012. Divergent carbon dynamics under climate change in forests with diverse soils, tree species, and land use histories. Ecosphere 3. https://doi.org/10.1890/ES12-00241.1 art110.
Schimel, J.P., Clein, J.S., 1996. Microbial response to freeze-thaw cycles in tundra and taiga soils. Soil Biol. Biochem. 28, 1061–1066. https://doi.org/10.1016/0038-0717(96)00083-1.
Scholten, R.C., Jandt, R., Miller, E.A., Rogers, B.M., Veraverbeke, S., 2021. Overwintering fires in boreal forests. Nature 593, 399. https://doi.org/10.1038/s41586-021-03437-y.
Seidl, R., Rammer, W., Scheller, R.M., Spies, T.A., 2012. An individual-based process model to simulate landscape-scale forest ecosystem dynamics. Ecol. Modell. 231, 87–100.
Sergueev, D., Tipenko, G., Romanovsky, V., Romanovskii, N., 2003. Mountain permafrost thickness evolution under influence of long-term climate fluctuations (results of numerical simulation). In: Proceedings of the VII International Permafrost Conference. Switzerland, pp. 21–25.
Shabaga, J.A., Bracho, R., Klockow, P.A., Lucash, M.S., Vogel, J.G., 2022. Shortened fire intervals stimulate carbon losses from heterotrophic respiration and reduce understorey plant productivity in boreal forests. Ecosystems. https://doi.org/10.1007/s10021-022-00761-w.
Sharkhuu, A., Sharkhuu, N., Etzelmüller, B., Heggem, E.S.F., Nelson, F.E., Shiklomanov, N.I., Goulden, C.E., Brown, J., 2007. Permafrost monitoring in the Hovsgol mountain region, Mongolia. J. Geophys. Res. 112, 2–06. https://doi.org/10.1029/2006JF000543.
Sharratt, B.S., 1992. Growing season trends in the Alaskan climate record 45, 124–127.
Short, K.C., 2021. Spatial wildfire occurrence data for the United States, 1992-2018 [FPA_FOD_20210617], 5th ed. Fort Collins, CO.
Silva, L.C.R., Anand, M., Leithead, M.D., 2010. Recent widespread tree growth decline despite increasing atmospheric CO_2. PLoS One 5, e11543. https://doi.org/10.1371/journal.pone.0011543.
Soetaert, K., Petzoldt, T., 2010. Inverse modelling, sensitivity and Monte Carlo analysis in R using package FME. J. Stat. Softw. 33, 1–28. https://doi.org/10.18637/jss.v033.i03.

Stewart, J.B., 1988. Modelling surface conductance of pine forest. Agric. For. Meteorol. 43, 19–35. https://doi.org/10.1016/0168-1923(88)90003-2.
Sturtevant, B.R., Scheller, R.M., Miranda, B.R., Shinneman, D., Syphard, A., 2009. Simulating dynamic and mixed-severity fire regimes: a process-based fire extension for LANDIS-II. Ecol. Modell. 220, 3380–3393. https://doi.org/10.1016/J.ECOLMODEL.2009.07.030.
Soil Survey Staff, Natural Resources Conservation Service, United States Department of Agriculture. 2020. U.S. General Soil Map (STATSGO2). Available online at https://sdmdataaccess.sc.egov.usda.gov. Accessed 10/05/2020.
Tebaldi, C., Mearns, L.O., Nychka, D., Smith, R.L., 2004. Regional probabilities of precipitation change: a Bayesian analysis of multimodel simulations. Geophys. Res. Lett. 31, 1–5. https://doi.org/10.1029/2004GL021276.
Turetsky, M.R., Mack, M.C., Hollingsworth, T.N., Harden, J.W., 2010. The role of mosses in ecosystem succession and function in Alaska's boreal forest. Can. J. For. Res. 40, 1237–1264. https://doi.org/10.1139/X10-072.
Ueyama, M., Iwata, H., Harazono, Y., 2018a. AmeriFlux BASE US-Rpf poker flat research range: succession from fire scar to deciduous forest, Ver. 6-5, AmeriFlux AMP, Dataset. 10.17190/AMF/1579540.
Ueyama, M., Iwata, H., Harazono, Y., 2018b. AmeriFlux BASE US-Uaf University of Alaska, Fairbanks, Ver. 9-5, AmeriFlux AMP dataset. 10.17190/AMF/1480322.
Ueyama, M., Iwata, H., Harazono, Y., 2014. Autumn warming reduces the CO_2 sink of a black spruce forest in interior Alaska based on a nine-year eddy covariance measurement. Glob. Chang. Biol. 20, 1161–1173. https://doi.org/10.1111/gcb.12434.
Ueyama, M., Iwata, H., Nagano, H., Tahara, N., Iwama, C., Harazono, Y., 2019. Carbon dioxide balance in early-successional forests after forest fires in interior Alaska. Agric. For. Meteorol. 275, 196–207. https://doi.org/10.1016/J.AGRFORMET.2019.05.020.
UN-ECE/FAO, 1985. The Forest Resources of the ECE Region. Europe, the USSR, North America, United Nations, Geneva, Italy.
USGS, 2020a. Alaska 2 Arc-second digital elevation models (DEMs) [WWW Document]. URL https://data.usgs.gov/datacatalog/data/USGS:4bd95204-7a29-4bd4-acce-00551ecaf47a.
USGS, 2020b. LANDFIRE 2020 Fuel Characteristic Classification System (FCCS) AK 2022 Capable Fuels [WWW Document]. URL https://landfire.gov/metadata/lf2020/AK/LA22_FCCS_220.html.
van Cleve, K., Chapin, F.S., Ruess, R.W., 2015. Bonanza Creek LTER: Tree inventory Data from 1989 to Present at Core Research Sites in Interior Alaska. Bonanza Creek LTER-University of Alaska Fairbanks, 0.6073/pasta/8366b043fbb4dfc220196425284d90a7.
Van Cleve, K., Chapin III, F.S., Flanagan, P.W., Viereck, L.A., Dyraess, C.T., 1986. Forest Ecosystems in the Alaskan taiga, a Synthesis of Structure and Function. Springer-Verlag, New York, NY.
Van Cleve, K., Dyrness, C.T., Viereck, L.A., Fox, J., Chapin, F.S., Oechel, W., 1983. Taiga in ecosystems interior Alaska. Bioscience 33, 39–44.
Van Cleve, K., Viereck, L.A., 1981. Forest succession in relation to nutrient cycling in the boreal forest of Alaska 185–211. 10.1007/978-1-4612-5950-3_13.
Vasiliev, A.A., Leibman, M.O., Moskalenko, N.G., 2008. Active layer monitoring in west Siberia under the CALM II program. In: Kane, DL, Hinkel, KM. (Eds.), Proceedings of the Ninth International Conference on Permafrost, p. 1820. Edited by.
Veraverbeke, S., Rogers, B.M., Goulden, M.L., Jandt, R.R., Miller, C.E., Wiggins, E.B., Randerson, J.T., 2017. Lightning as a major driver of recent large fire years in North American boreal forests. Nat. Clim Chang. 7, 529–534. https://doi.org/10.1038/NCLIMATE3329.
Viereck, L.A., 1982. Effects of fire and firelines on active layer thickness and soil temperatures in interior Alaska. In: Proceedings of the 4th Conference Permafrost Conference, The Roger J.E. Brown Memorial Volume. National Research Council of Canada. Ottawa, Canda, pp. 123–134.
Viereck, L.A., Werdin-Pfisterer, N.R., Adams, P.C., Yoshikawa, K., 2008. Effect of wildfire and fireline construction on the annual depth of thaw in a black spruce permafrost forest in interior Alaska: a 36-year record of recovery. Eds.. In: Kane, Douglas L., Hinkel, Kenneth M. (Eds.), Proceedings of the Ninth International Conference on Permafrost. Fairbanks, AK, pp. 1845–1850. June 29-July 3, 2008.
Viglas, J.N., Brown, C.D., Johnstone, J.F., 2013. Age and size effects on seed productivity of northern black spruce. Can. J. For. Res. 43, 534–543. https://doi.org/10.1139/cjfr-2013-0022.
Vogel, J.G., Valentine, D.W., Ruess, R.W., 2005. Soil and root respiration in mature Alaskan black spruce forests that vary in soil organic matter decomposition rates. 10.1139/X04-159.
Walker, A.P., De Kauwe, M.G., Bastos, A., Belmecheri, S., Georgiou, K., Keeling, R.F., McMahon, S.M., Medlyn, B.E., Moore, D.J.P., Norby, R.J., Zaehle, S., Anderson-Teixeira, K.J., Battipaglia, G., Brienen, R.J.W., Cabugao, K.G., Cailleret, M., Campbell, E., Canadell, J.G., Ciais, P., Craig, M.E., Ellsworth, D.S., Farquhar, G.D., Fatichi, S., Fisher, J.B., Frank, D.C., Graven, H., Gu, L., Haverd, V., Heilman, K., Heimann, M., Hungate, B.A., Iversen, C.M., Joos, F., Jiang, M., Keenan, T.F., Knauer, J., Körner, C., Leshyk, V.O., Leuzinger, S., Liu, Y., MacBean, N., Malhi, Y., McVicar, T.R., Penuelas, J., Pongratz, J., Powell, A.S., Riutta, T., Sabot, M.E.B., Schleucher, J., Sitch, S., Smith, W.K., Sulman, B., Taylor, B., Terrer, C., Torn, M.S., Treseder, K.K., Trugman, A.T., Trumbore, S.E., Mantgem, P.J., Voelker, S.L., Whelan, M.E., Zuidema, P.A., 2021. Integrating the evidence for a terrestrial carbon sink caused by increasing atmospheric CO_2. New Phytol. 229, 2413–2445. https://doi.org/10.1111/nph.16866.
Walker, D.A., Jia, G.J., Epstein, H.E., Raynolds, M.K., Chapin, I.S., Copass, C., Hinzman, L.D., Knudson, J.A., Maier, H.A., Michaelson, G.J., Nelson, F., Ping, C.L., Romanovsky, V.E., Shiklomanov, N., 2003. Vegetation-soil-thaw-depth relationships along a low-arctic bioclimate gradient, Alaska: synthesis of information from the ATLAS studies. Permafr. Periglac. Process. 14, 103–123. https://doi.org/10.1002/ppp.452.
Walsh, J.E., 2014. Our changing climate. Eds.. In: Melillo, J.M., Richmond, T.C., Yohe, G. W. (Eds.), Climate Change Impacts in the United States: The third National Climate Assessment. U.S. Global Change Research Program, pp. 19–67. https://doi.org/10.7930/J0KW5CXT.
Wendler, G., Shulski, M., 2009. A century of climate change for Fairbanks, Alaska. Arctic 62, 295–300.
Wolken, J.M., Hollingsworth, T.N., Rupp, T.S., Chapin, F.S., Trainor, S.F., Barrett, T.M., Sullivan, P.F., Mcguire, A.D., Euskirchen, E.S., Hennon, P.E., Beever, E.A., Conn, J.S., Crone, L.K., D'Amore, D.V., Fresco, N., Hanley, T.A., Kielland, K., Kruse, J.J., Patterson, T., Schuur, E.A.G., Verbyla, D.L., Yarie, J., 2011. Evidence and implications of recent and projected climate change in Alaska's forest ecosystems. Ecosphere 2. https://doi.org/10.1890/ES11-00288.1.
Yarie, J., Viereck, L., Cleve, K.Van, Adams, P., 1998. Flooding and ecosystem dynamics along the Tanana River: applying the state-factor approach to studies of ecosystem structure and function on the Tanana River floodplain. Bioscience 48, 690–695.
Yi, S., McGuire, A.D., Harden, J., Kasischke, E., Manies, K., Hinzman, L., Liljedahl, A., Randerson, J., Liu, H., Romanovsky, V., Marchenko, S., Kim, Y., 2009. Interactions between soil thermal and hydrological dynamics in the response of Alaska ecosystems to fire disturbance. J. Geophys. Res. Biogeosci. 114 https://doi.org/10.1029/2008JG000841.
Yoshikawa, K., Bolton, W.R., Romanovsky, V.E., Fukuda, M., Hinzman, L.D., 2003. Impacts of wildfire on the permafrost in the boreal forests of interior Alaska. J. Geophys. Res. Atmos. 108 https://doi.org/10.1029/2001jd000438.
Yoshikawa, K., Hinzman, L.D., 2003. Shrinking thermokarst ponds and groundwater dynamics in discontinuous permafrost near Council, Alaska. Permafr. Periglac. Process. 14, 151–160. https://doi.org/10.1002/PPP.451.
Zha, J., Zhuang, Q., 2021. Quantifying the role of moss in terrestrial ecosystem carbon dynamics in Junrong Zha and Qianlai Zhuang. Biogeosci. 18, 6245–6269. https://doi.org/10.5194/bg-18-6245-2021.
Zhang, Y., Carey, S.K., Quinton, W.L., Janowicz, J.R., Pomeroy, J.W., Flerchinger, G.N., 2010. Comparison of algorithms and parameterisations for infiltration into organic-covered permafrost soils. Hydrol. Earth Syst. Sci. 14, 729–750. https://doi.org/10.5194/hess-14-729-2010.
Zuur, A.F., Ieno, E.N., Walker, N.J., Saveliev, A.A., Smith, G.M., 2009. Zero-Truncated and Zero-Inflated Models for Count Data. In: Mixed effects models and extensions in ecology with R. Statistics for Biology and Health. Springer, New York, NY. https://doi.org/10.1007/978-0-387-87458-6_11.